6G Beamforming Antenna-in-Package

Improving Efficiency using Direct Impedance Matching

Roeland Kooij

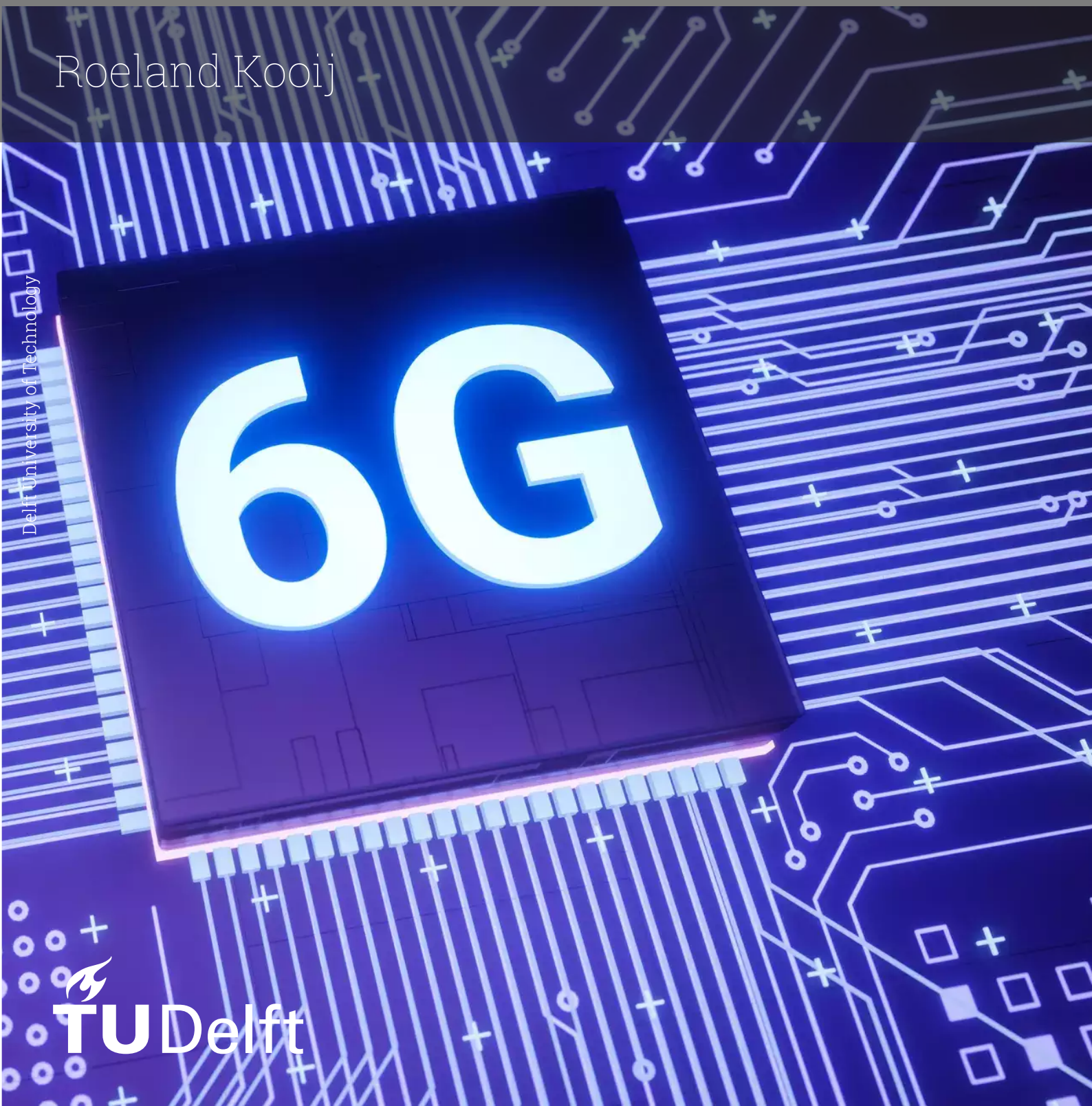

Delft University of Technology

TU Delft

6G Beamforming Antenna-in-Package

Improving Efficiency using Direct Impedance Matching

by

Roeland Kooij

to obtain the degree of Master of Science

at the Delft University of Technology,

to be defended publicly on Thursday September 28, 2023 at 13:00 AM.

Student number:	4313801	
Project duration:	December 5, 2022 – September 5, 2023	
Thesis committee:	Prof. DSc. A. Yarovoy,	TU Delft, supervisor
	Dr. Y. Aslan,	TU Delft, daily supervisor
	Dr. S.M. Alavi,	TU Delft, external committee member
	Ir. K. Giannakidis,	NXP Semiconductors, daily supervisor

TU Delft

Abstract

As the world is getting used to 5G technology, 6G is already on the horizon. With the ultimate goal of very low latency communication and Tbps data rates, 6G supports new wireless technologies such as virtual and augmented reality and autonomous driving. In this new generation of wireless communication, high frequencies up to 100 GHz are used which causes antenna arrays to shrink to the size of a post stamp. Antenna-in-Package (AiP) is an emerging technology that integrates these antennas directly in the packaging material of IC's. This brings the benefit of high level of integration, making beamforming IC's an all in one system for communications. Despite this, high integration also comes with challenges. These small antenna systems generate heat on a small footprint which emphasizes the need for a low-loss, efficient system. Moreover, free-space path loss is proportional to frequency so high radiated power is needed, further emphasizing the need for improved efficiency. Lastly, space inside the IC and package material is limited which requires compact solutions for the system's components. Literature has shown that PA-antenna co-design can reduce losses at the PA-antenna interface by matching the antenna impedance to the impedance of the power amplifier, omitting the need for lossy impedance matching networks. This method, called direct impedance matching, has shown to improve power added efficiency (PAE) in antenna systems with single radiating elements and fixed linear arrays. Nevertheless, the advantage of direct impedance matching has not yet been demonstrated for phased array antennas with active beam forming/steering.

This work demonstrates a novel analysis of PA-antenna co-design at 96 GHz using a 8x8 cavity-backed dual-polarized pin-fed stacked patch array. Two versions of this antenna array are designed in Ansys HFSS, one with an antenna impedance of 50 Ω, the benchmark, and one with a lower impedance of 25 Ω. Both designs are made on a custom package laminate stack-up and are compatible with pin-fed AiP technology. Using Keysight ADS, the antenna designs are co-simulated with an RF front-end circuit comprised of a single tone AC signal, ideal 1-64 channel power divider, ideal continuous phase shifters and realistic SiGe Class A cascode power amplifiers. In this setup, the 50 Ω reference antenna is connected to the PA's with a matching network in between. Because the 25 Ω antenna array matches the optimal output impedance of the PA, it is directly connected. The performance of both antenna arrays are compared, with the focus on PAE and radiation characteristics. The results show that by going for a directly matched antenna the PAE of the system increases by 15.6% for a broadside beam and 30.4% with a scanned beam ($\theta = 45°, \phi = 45°$). EIRP for broadside and scanned beams increased from 50.3 W to 56.3 W and from 31.1 W to 37.9 W respectively. Bandwidth, gain, radiation efficiency and side-lobe levels were similar in both arrays but the 25 Ω antenna had 4 dB higher levels of cross-polarized radiation and a 4 dB stronger back-lobe behind the antenna. The advantage of higher efficiency and radiated power outweighs these drawbacks and makes direct impedance matching a good design strategy for 6G beamforming AiP technology.

Acknowledgements

With the completion of my thesis I would like to thank all the people who have supported me throughout this journey.

First of all I would like to thank Dr. Yanki Aslan, who gave me the amazing opportunity to do my thesis in collaboration with NXP Semiconductors Eindhoven. I appreciate the guidance and support you gave me during my thesis project. Your apt replies to my questions were always extensive and helpful. It was a pleasure to have you as my daily supervisor.

I would like to thank Prof. DSc. Alexander Yarovoy for his support during my time at the Microwave Sensing, Signals and Systems research group. You helped me overcome big hurdles during the last stages of my master's program. Graduating would not have been possible without your help.

In addition I express my sincere gratitude to the employees of NXP Semiconductors who have guided me during my thesis project. Thank you Konstantinos Giannakidis, my daily supervisor at NXP. You have taught me so much about working at a company, and introduced me to new ways of conducting research. Mustafa Acar and Jasper Pijl, despite not being supervisors of mine, were always ready for questions and brainstorms. Thank you both for your interest and involvement in my project.

Last but not least I would like to thank my family who have always supported me throughout my long journey at the university. Thanks to you all I never gave up on this endeavor, you gave me the motivation to finish what I started.

Roeland Kooij
Delft, September 2023

Contents

1 Introduction

In this chapter, first the concept of Antenna-in-Package (AiP) technology is introduced, forming the motivation of this thesis. Then, challenges for 6G AiP designs are explained and the research problem is formulated. From this, the thesis project is introduced along with the research scope and goals. A literature review is presented, followed by the system requirements and research approach. To finish the introduction, an outline of the thesis structure is given.

1.1. Motivation

Wireless communication has been an integral part of our society. Technology trends, such as high speed cellphone communication, Wi-Fi networks, smart electronics, internet of things (IoT) devices, advanced driver assistance systems (ADAS), virtual reality and augmented reality has pushed wireless communication hardware to new boundaries. To meet the demands of these applications, a very high speed, low latency communication channel is required. The capacity of the channel is proportional to the bandwidth of the channel, according to the Shannon-Hartley theorem:

$$C = B * log_2\left(1 + \frac{S}{N}\right) \tag{1.1}$$

To achieve high bandwidth in the design of radio hardware, the simplest solution is to move to high frequencies. This increases the bandwidth while allowing the percent bandwidth of the system to remain unchanged. As such, existing design principles that have been used for years at lower frequencies can be scaled down to match the frequency needs of today.

With 5G technology currently widely adopted, high speed communication has already been established at mmWave frequencies. As the name suggests, the high-band of 5G, operating from 24-47 GHz, uses wavelengths of about 10 mm. Because antenna dimensions are proportional to the wavelength, antenna designs have been shrinking while the industry is pushing for higher frequencies.

With smaller antennas comes the opportunity of high integration with radio frequency (RF) hardware. Previously we have already seen integration on printed circuit board (PCB) level with the wide adoption of microstrip patch antennas. These antennas are made on the PCB by making patches with a microstrip metal layer on top of the PCB substrate, with a ground plane metal layer below the substrate. Using this method, an RF integrated circuit (IC) on the board can feed an antenna on the same board by means of an antenna feed connection. An even higher level of integration can be achieved by fabricating the antenna right into the IC package. This method is called **Antenna-in-Package (AiP)**, an example of this antenna type is illustrated in Figure 1.1 [1].

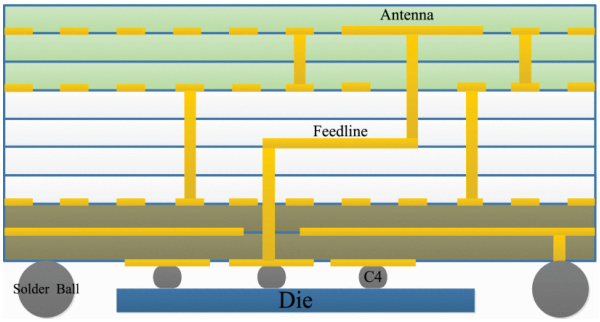

Figure 1.1: Cross-section of Antenna-in-Package design [1]

With 5G now an established technology, the industry is already looking towards 6G. Frequencies for this new generation are going as high as 100 GHz. With a wavelength of only 3 mm at this frequency, it is possible to fit an entire planar array antenna into the IC-package making AiP technology an attractive solution.

Establishing a communication link at frequencies as high as 100 GHz comes with a new set of challenges. Most notably, by observing the Friis transmission formula (see equation 1.2), decreasing the wavelength while keeping other variables fixed causes a significant drop in received power.

$$\frac{P_r}{P_t} = D_t D_r \left(\frac{\lambda}{4\pi d}\right)^2 \tag{1.2}$$

The term attributed to this loss is called free-space path loss (FSPL). For increasing distance between the transmitter and the receiver, the signal loses power due to spreading of the electromagnetic energy according to the inverse-square law. Confusingly, the wavelength dependence of the FSPL has nothing to do with the communication path but is rather attributed to the decrease in antenna size at small wavelengths, leading to a smaller aperture to capture radiated power. As a result, given equal received power and antenna directivity, a high frequency communication link requires much higher transmit power to achieve an acceptable signal to noise ratio (SNR). To overcome this issue, multiple antennas can be combined as a planar array to increase the antenna aperture, leading to a much higher directivity of the radiation. This method is called beam forming, and by adding phase shifts on the individual elements, this beam can be steered, forming what is called phased arrays. Examples of phased array antennas are shown in Figures 1.2a and 1.2b.

(a) 5G phased array by NXP Semiconductors

(b) 5G dielectric resonator antenna array by Antenna Company

Figure 1.2: Examples of phased array antennas with high directivity

1.1.1. Problem Formulation

The high level of integration that comes with AiP brings the benefit of having a much shorter interconnect between the antenna and the RF-IC, which limits spurious radiation and power losses from the feed line. Additionally, the RF system can be made as an all-in-one product which increases its value in the commercial market. As a downside, this high level of integration places components close to each other which as a main concern brings problems with temperature management [2]. IC packages of high heat producing chips are often fitted with a cooling device. Common examples of this are the CPU and GPU of computers. In phased array systems, these cooling devices have also been shown to be effective [3]. With an RF-IC that supports arrays, multiple channels need amplification, and amplifiers generate heat during operation. With an antenna array built into the package, a cooling device can no longer be fitted on top of the package and heat is trapped between the IC and the antenna. High operation temperatures lead to many problems, such as semiconductor failure and expansion of materials leading to warping structures. As a solution, the IC is cooled from the backside of the PCB using heatsinks. The antenna itself also contributes to some extent in drawing away heat from the amplifiers.

The best solution to manage heat is to reduce heat production in the first place, which calls for higher **efficiency**, especially in high power components of the IC. In addition, by increasing power efficiency a higher radiated power can be achieved. This helps to overcome the challenge of FSPL, results in a higher SNR and increases the quality of the wireless link. To do this we have to identify sources of major power loss:

- **Low efficiency of the power amplifier (PA):** At the frequency of 100 GHz, high efficiency power amplifiers are particularly challenging to design. Simple amplifier designs are used such as the biased class A amplifier, or the push-pull configuration of class B. Class A amplifiers, despite being mostly linear and harmonically stable, are inherently inefficient due to a bias current that continuously dissipates power in the transistor. A basic common emitter class A amplifier can theoretically only reach a max efficiency of 25 %, by coupling the output with a transformer, this can be increased to 50 %. Realistically the efficiency is even lower, as is demonstrated in [4] with a W-band cascode SiGe BiCMOS power amplifier that peaks at an efficiency of 17.2% at 93 GHz.
- **Power loss in lossy impedance matching network at the PA-feedline interface:** To prevent signal reflections at the PA output, the feedline to the antenna has to match the output impedance of the PA. The feedline in most cases has a characteristic impedance of 50 Ω, while PA's often have a lower impedance at the output. An impedance matching network can transform the impedance of the PA to match that of the feed line. Implementations vary from lumped capacitors and inductors to transmission line stubs and quarter wave transformers. The problem is that this impedance matching is done at the output of the PA, and thus high currents run through the lossy components of the network.
- **Losses in the antenna feed:** Antenna feeds can become fairly long for large arrays. High power signals run through the feed and attenuate over distance due to dielectric and conductor losses. If the feed contains many transitions and different impedances along the line, reflections can play a role too.
- **Low radiation efficiency of the antenna:** Patch antennas generally have lower radiation efficiency compared to wire and aperture antennas due to dielectric losses. Especially wideband patch antennas, which sit on a thick substrate layer e.g. $h = \lambda/20$ can suffer from surface waves, trapping radiation inside the dielectric.

Clearly, antenna impedance plays a large role in the amount of power loss in the RF system. This power loss is surprisingly still accepted in some RF-IC designs for 6G frequencies, where the IC is subjected to standardized 50 Ω antenna impedance [5], [6]. A solution to this problem is called **direct impedance matching**, where impedances of interconnected components are matched by design instead of using a matching network. This principle is shown in Figure 1.3

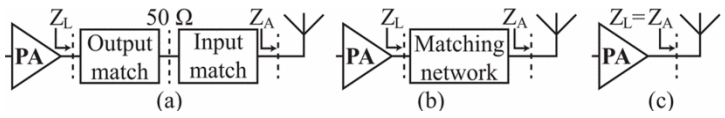

Figure 1.3: schematic of (a) matching with 50 Ω interface, (b) single matching network, (c) direct matching. [7]

1.2. Research Scope and Goals

The goal of this thesis is to design a dual-polarized 8x8 coaxial probe-fed antenna array using AiP technology for a 96 GHz 6G beamforming RF-IC at an impedance that matches the PA output. **Using PA-antenna co-design, the aim is to reduce losses by omitting the matching network at the PA output.** By comparing a 25 Ω antenna design to a 50 Ω state-of-the-art benchmark, this thesis aims to show that such an antenna design is feasible and has merit for AiP technology at 96 GHz. The project has been done in collaboration with NXP Semiconductors in Eindhoven.

The project is bound to the following scope:

- The antenna array will be designed on the package laminate technology supplied by NXP Semiconductors. This limits the degree of freedom in the design in terms of material choice, dimensions, tolerances and geometries.
- The design has to meet certain performance requirements to be considered feasible. These requirements include: Radiation efficiency, mismatch losses, bandwidth, cross-polarization levels, port isolation and scanning range.
- The design process will be done using EM-solver simulation tools. Because the design asks for an 8x8 array, accurate simulations will require large amounts of memory and computing time. This slows down the iterative design process.
- The antenna feeding network between the power amplifiers and the antenna elements of the array is left outside the scope of this thesis because it is too complex to design within the project's time frame.

1.3. Literature Review

A review of several articles on PA-antenna direct impedance matching are presented here. The goal of this literature review is to investigate the advantages and disadvantages of direct impedance matching, the feasibility of a directly matched antenna design, and the novelties of the proposed project.

1.3.1. Direct impedance matching

E.B. Abdallah et al. (2015) in [8] have demonstrated a directly matched antenna using a small patch antenna design for 0.9 GHz. The patch antenna design is basic and thus only has a 1.1% bandwidth. The feed is a coaxial probe that terminates into a disc that is capacitively coupled to the patch. This allows for tuning of the input impedance and makes the antenna electrically small with a low impedance of 2.8 + 0.7j Ω. In their research, the antenna is directly connected to a silicon-on-insulator LDMOS class A amplifier, and power added efficiency (PAE) of the amplifier was measured. The PAE with their new antenna design was 45%, while their reference measurement with a 50 Ω antenna was 33%. A drawback is that their antenna design is narrow-band, and has a low radiation efficiency outside of the resonance frequency. Additionally, the feeding technique requires very accurate placement of the capacitive coupling disc lowering the feasibility of the antenna design.

W.-C. Liao et al. (2018) in [9] presented a design flow for directly matched antennas for 5G applications. In the paper a GaN high-electron-mobility transistor (HEMT) class A amplifier was found to be optimized in terms of PAE at 30 GHz for low resistance loads. A design strategy for an electrically small loop antenna is presented where an antenna of 5 + 500j Ω was directly connected to the PA for a PAE of 15%. The authors found a significant trade-off between radiation efficiency of the antenna and PAE of the amplifier. Radiation efficiency was found to be low at 26% due to the radiation resistance becoming small with respect to the loss resistance.

W.-C. Liao et al. (2019) in [10] continued their research on direct impedance matching by presenting a novel PA-antenna co-design. In this design a GaN HEMT amplifier is integrated into a 20 GHz slot antenna by directly connecting the transistor source to one side of the slot and the transistor drain via a bondwire and capacitor to the other side of the slot, see Figure 1.4. The antenna is entirely made from metal and also serves as a heatsink for the PA.

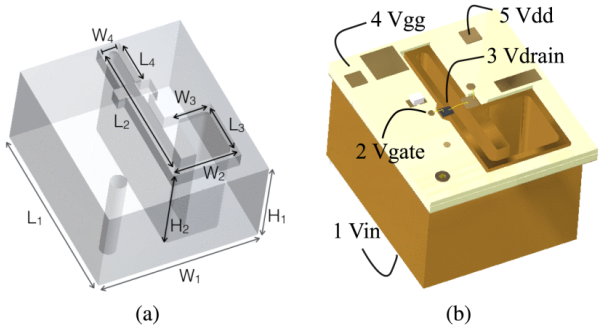

Figure 1.4: Geometry of 20 GHz slot antenna with integrated power amplifier. [10]

PAE of the amplifier was found to be optimal for a 17 + 46j Ω load. The antenna was designed to match this impedance and simulations showed a 10% increase in PAE when using this antenna compared to a 50 Ω load with a lossy microstrip-line stub-based impedance-matching network.

S. N. Nallandhigal and K. Wu (2018) in [11] present a novel design of a linear array of patch antennas with amplifiers in between the elements. In this topology, an RF signal enters one side of the array and passes through all of the elements. 73% of the power is radiated by the antenna elements and the rest is passed on down the chain with amplification in between. The transistors (class A, HJ-FET) are directly connected to the antennas without matching networks. A schematic of the design is given in Figure 1.5.

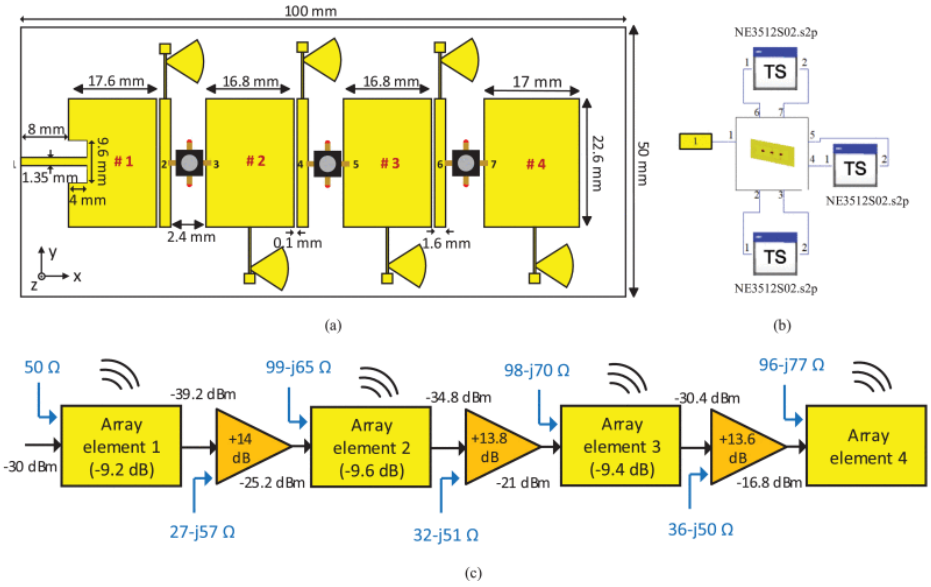

Figure 1.5: Schematic of 5 GHz antenna 1x4 antenna array with integrated amplifiers. [11]

Figure 1.5 shows the power to the antenna elements grows as the signal passes through the array. The last element contributes the most to the overall radiation of the array. The beam is also offset at 34° from broadside because of a phase shift between elements.

H. Kim, I. Yoon and Y. J. Yoon (2005) in [12] demonstrated a slot antenna at 5.4 GHz that was directly matched to a class B/F GaAs FET amplifier. Besides omitting a PA output impedance matching network, they also omitted a harmonic tuning network by integrating it into the antenna design. The antenna was designed with an impedance of 18.4 - 17.5j Ω at the center frequency, 0.5 + 8.5j Ω for the second harmonic (approximate short circuit) and 330 + 800j Ω for the third harmonic (approximate open circuit). Using these techniques, PAE of the amplifier reached 67.5% and reduced the size of the RF front-end structure by 43% compared to conventional efficient class F amplifier designs. The same technique

was applied in [13] for WiFi applications at 2.4 GHz using an L-shaped microstrip antenna. Their antenna design is tuned to 22.4 + j1.9 Ω at the center frequency and at second harmonic, 4.8 GHz the impedance is 0.3 + j19.4 Ω. Similar results were also obtained in [14] using a triple slot antenna design for 3.5 GHz. Using impedances of 12.9 - 6.9j Ω, 1.4 - 16j Ω and 1011 - 204j Ω for the fundamental, second and third harmonic frequencies respectively, PAE of the system was found to improve from 52% to 65.9%.

1.3.2. Summary

To summarize the research from the discussed literature, Table 1.1 shows the specifications that all of the literature reported. For the antenna impedance, only the impedance at the fundamental frequency is shown.

Table 1.1: Summary of literature review

Antenna Design	f (GHz)	Antenna impedance (Ω)	Peak PAE (%)
Small patch	0.9	2.8 + 0.7j	33 ->45
Small loop	30	5 +500j	15
Slot	20	17 +46j	24.8 ->34.8
Series-fed patches with PA's in between	5	99 - 65j	19
Slot with L/C stub	5.4	18.4 - 17.5j	64 ->67.5
L-shaped microstrip	2.4	22.4 + 1.9j	62
Triple slot	3.5	12.9 - 6.9j	52 ->65.9

M. de Kok et al. (2022) in [7] reviewed the current state of direct impedance matching for PA-antenna co-designs. Their findings were that antenna designs that match an amplifier's ideal load impedance have merit when looking at key parameters such as PAE and output power. Despite this, current examples of direct impedance matched antennas have only demonstrated its use for either single radiating elements or fixed array configurations. For phased arrays with active beam steering there are no documented studies that demonstrate direct impedance matching. With significant mutual coupling effects in these arrays, direct impedance matching is particularly challenging due to variation of antenna impedance under scanning conditions. Moreover, direct impedance matching has not yet been done in AiP designs with pin-fed radiators.

1.3.3. Novelties

Direct impedance matching has been proven to be a successful design approach for improving RF-system efficiency. Although direct impedance matching has yet to be studied at 6G frequencies, the design approach is deemed feasible as long as the antenna design is kept simple and adheres to requirements and tolerances for fabrication. This thesis introduces the following novelties:

- For the first time, direct impedance matching is applied to a planar phased array antenna with active beam forming/steering.
- The possibility of dual polarization for directly matched antennas will be shown in this study.
- A direct impedance matched antenna is made compatible with industry-standard pin-fed antenna-in-package technology.
- For the first time a direct impedance matched antenna array is designed using cavity backed elements to address varying impedance under scanned conditions.

1.4. System Requirements and Research Approach

To investigate whether a PA-antenna co-design is feasible for 96 GHz and provides a reduction of power loss in the antenna system, a novel design of an antenna array has to be made that matches the ideal output impedance of the PA. The PA used in this research performs optimally for a 25 Ω load. The approach is to design two antenna arrays, one reference design with a 50 Ω impedance and one novel design with a 25 Ω impedance. Both antenna designs will then be simulated by connecting them to an RF beamforming circuit, with realistic PA models supplied by NXP Semiconductors. To achieve

this, the research has been split into three phases. In this section the approach for each phase will be explained in detail.

1.4.1. Phase one: Antenna element design.

In the first phase, an antenna element will be designed. First, the reference 50 Ω design is made, then a 25 Ω design. Both designs should adhere to the requirements listed below:

- The center frequency of the antenna is 96 GHz.
- The antenna has a bandwidth of $\sim$20%. This is a higher bandwidth than the RF-IC supports but this acts as a safety margin to account for fabrication error and inaccuracies with the simulation model.
- The bandwidth is defined as the -10 dB crossover points in the return loss of the antenna. Although similar to the last point, as a safety margin a lower return loss limit of -15 dB is desirable.
- Cross-polarization levels with respect to the co-polarized radiation should be around -20 dB
- The design is implemented on package laminate substrate supplied by NXP Semiconductors
- The antenna is dual linearly polarized and has two antenna feeds for each polarization axis.
- The element is square ($W = L$) and the sides cannot be bigger than $\lambda/2$

1.4.2. Phase two: Antenna array design.

In this phase, 8x8 antenna arrays are designed. The designs are based on the unit cells from phase one, requiring additional tuning. Requirements from the antenna elements apply to the array designs as well. Because beamforming arrays introduce new parameters, additional requirements have to be defined:

- The beam can be scanned by introducing a phase shift on the input signal of the antenna elements. The scanning range is defined as the amount of scanning that can be done while still meeting the bandwidth requirements and would ideally be $\pm 50^{\circ}$ in both E-plane and H-plane.
- Mutual coupling between antenna elements should be kept as low as possible. As a goal, -20 dB of port coupling between elements is acceptable.
- Spacing between elements should be adequately close so there are no grating lobes over the desired scanning range, over all frequencies in the bandwidth of operation
- Radiation efficiency of the entire array should be at least 85%. Ideally the radiation efficiency for both the 50 Ω reference design and the 25 Ω design will be more or less the same.

Both phase one and phase two will be designed using Ansys HFSS, an EM solver using the Finite Element Method (FEM). Simulations are carried out on a High Power Computing (HPC) server, where resources of up to 200 GB of memory and 24 computing cores can be used.

1.4.3. Phase three: Antenna system analysis.

In this phase the antenna arrays are connected to RF-circuit components to investigate whether the 25 Ω antenna design provides benefits with respect to the reference design. The main goal is to show the effects on PAE of the PA, similar to the literature reviewed. In addition, radiation performance is also assessed. This is done in a simulation environment using Advanced Design System (ADS). The geometry of the antenna designs from HFSS will be replicated in ADS and simulated again with a FEM EM solver. ADS then provides the ability to co-simulate a circuit connected to the antenna and give a complementary solution of the antenna radiation. To make this phase of the research feasible within the time-frame of the project, the following requirements are defined for this part:

- The antenna system is simulated using a single tone excitation at the center frequency of 96 GHz.
- The RF circuit has 64 channels to excite every element in the array. The channels are connected to a single source using an ideal (lossless) Wilkinson power divider.
- Each channel is fitted with an ideal phase shifter for beam steering
- Each channel is fitted with a realistic power amplifier model supplied by NXP Semiconductors.

- For the 50 Ω reference design, a realistic model of a matching network is connected between the PA output and the antenna input (for each channel), for the 25 Ω design the antenna elements are directly connected to the amplifiers.

1.5. Thesis outline

The structure of this thesis follows the aforementioned design phases of the research method:

Chapter 2 presents the design of a unit cell antenna element on package laminate substrate. First a reference design is made with an input impedance of 50 Ω. The design process is explained step by step. The coaxial probe feed is explained as well as the stacked patch configuration to extend the bandwidth. The final design of the 50 Ω reference antenna is a dual-polarized probe-fed stacked patch antenna. A novel 25 Ω direct impedance matched design is made with a similar design strategy as the reference. The problem of probe reactance is identified and multiple solutions are presented. A combination of cavity-backing using via walls along with a thinner bottom substrate made it possible to tune the antenna to 25 Ω. Both antenna elements are compared in terms of impedance, bandwidth and radiation performance.

In Chapter 3 a 25 Ω and 50 Ω antenna array of size 8x8 is presented. The designs are based on unit cell designs from the previous chapter with additional tuning. Both arrays feature cavity backed elements and follow the same design principals. A simulation approach is explained to get accurate results within reasonable amount of time. Both antenna arrays are compared in terms of impedance, bandwidth, scanning capability and radiation performance. In addition, mutual coupling is also studied by observing port-coupling data between neighbouring antenna elements. For the radiation performance, focus is put on co-polarized and cross-polarized gain, side lobe level and beam width.

Chapter 4 presents a circuit- and electromagnetic co-simulation of the antenna arrays in an RF beam-forming circuit. An overview of the circuit is given and each part is explained. A brief explanation on the PA is given, along with a detailed description of the matching network for 50 Ω connections. To assess the performance of the system, Power Added Efficiency (PAE), AM/AM distortion and AM/PM distortion is calculated. A power sweep simulation on the signal input power at the PA was done to reveal the 1 dB compression point. Then, 6 dB of headroom to the 1 dB compression point was given for a final simulation, resulting in roughly 1 mW of signal input power in each channel. The simulation results for both 50 Ω and 25 Ω arrays are compared and summarized in a table. The table contains radiation results from Chapter 3 for a more complete comparison.

Lastly, in Chapter 5 a summary is given on the contents of this thesis, along with a conclusion and suggestions for future research.

2

Antenna Unit Cell Design

The goal is to design an antenna of 8x8 unit cells in an array. This process starts with a design of the unit cell. This chapter covers the design process of an antenna element that is to be used in a planar array configuration. Complementary background information is given, along with design choices and simulation results. The antenna element is designed and tested in HFSS.

2.1. Background Information: Microstrip Patch Antenna

A microstrip patch antenna is made by placing a thin patch of a metal strip above a groundplane, separated by a dielectric substrate. The antenna, shown in Figure 2.1 has two radiating slots at $y = 0$ and $y = L$ with area $W * h$. The radiation from these slots combine to form a broadside radiation pattern that has a maximum normal to the patch surface. Typical patch antenna designs feature very thin ($t_m \ll \lambda_0$, λ_0 being the wavelength in vacuum) metal patches, often made from copper, that have high conductivity. The dielectric substrate can have a large range of permittivities ($2 < \epsilon_r < 12$) and height ($0.003\lambda_0 \leq h \leq 0.02\lambda_0$), although low dielectric permittivity and large height is desirable for high radiation efficiency and larger bandwidth [15]. Patch antennas can come in all kinds of shapes but the most common shape is rectangular, as illustrated in Figure 2.1. This type of patch antenna is relatively easy to analyse, design and manufacture, while offering good radiation characteristics with low cross polarization. Because of their design simplicity, small size and good integration with PCB circuitry, microstrip patch antennas are the number one choice for compact antenna arrays.

As can be seen in Figure 2.1b the field below the patch is a standing wave, with a null at the center of the patch. This is the dominant TM_{010} mode and it implies that the current at the center is maximum and the voltage is zero. Because the field behaves as a standing wave, the input resistance of the patch changes according to the position of the feed (y_0). For a rectangular patch the normalized input resistance follows a cosine-squared distribution, shown in Figure 2.2.

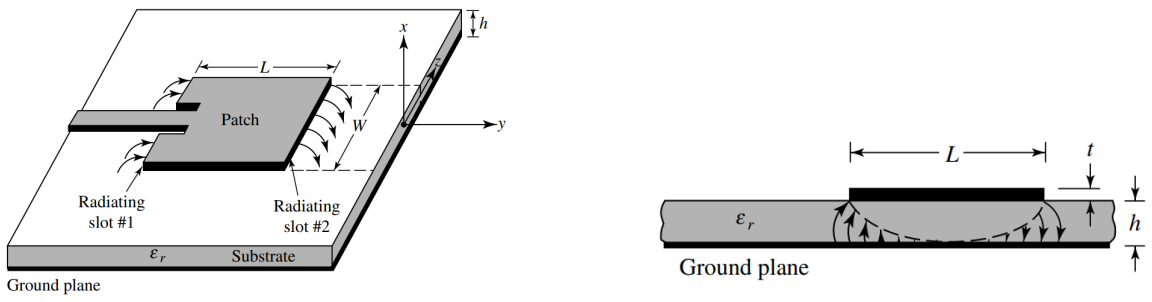

(a) Microstrip patch antenna

(b) Side view

Figure 2.1: Microstrip patch antenna [15]

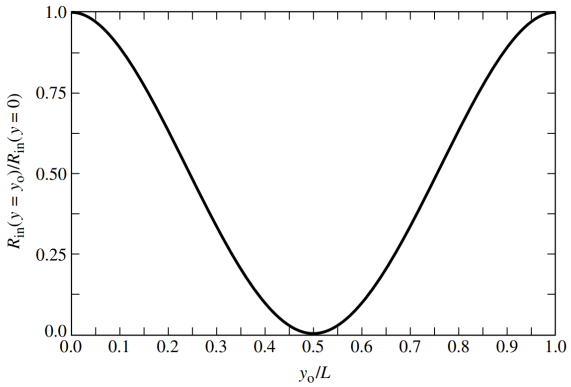

Figure 2.2: Normalized input impedance of patch antenna vs. feed location

2.1.1. Coaxial Probe Feed

To make the patch antenna radiate, resonating modes have to be excited in the cavity below the patch. An antenna feed has to provide energy to the patch, which can be done in several ways. The most common feeds include: inset microstrip feed line, coaxial probe feed, proximity-coupled feed and aperture-coupled feed. This section will focus on the coaxial probe feed because it is the feed method used for this thesis project.

The coaxial probe feed consists of a coaxial line below the ground plane and a probe protruding the substrate. The shield of the coaxial line connects to the groundplane while the inner conductor of the coax extends as a probe through the subtrate, and connects to the patch, see Figure 2.3. Because the antenna input impedance is distributed along different lengthwise feed locations (see Figure 2.2), this property can be used to tune the antenna impedance by positioning the feed at different locations. The impedance will be high towards the radiating edge of the patch, and zero at the center. The coaxial feed has a characteristic impedance Z_0, determined by the inner conductor's diameter d, the inner diameter of the shield D and the dielectric permittivity ϵ_r, see equation 2.1

$$Z_0 \approx \frac{138}{\sqrt{\epsilon_r}} log_{10}\left(\frac{D}{d}\right) \tag{2.1}$$

This characteristic impedance of the feed line is usually 50 Ω for which a sweet spot on the patch exists that matches this impedance.

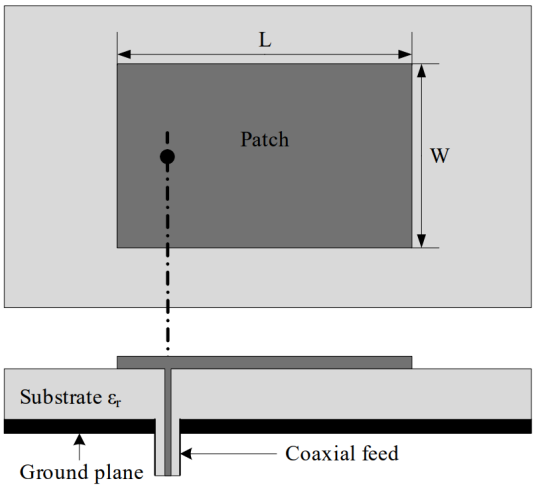

Figure 2.3: Coaxial probe feed for microstrip patch antenna [16]

2.1.2. Equivalent Circuit Model

The input impedance of a probe-fed patch antenna can be modelled using lumped circuit components, see Figure 2.4.

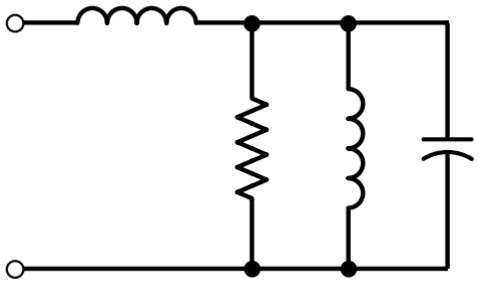

Figure 2.4: Equivalent circuit of a probe-fed microstrip patch antenna [15]

The patch has a resonant frequency, where the real impedance maximises and imaginary impedance crosses zero. This is similar to an RLC resonator, and thus we can model the patch as a parallel RLC. The resonator is connected in series to an inductor which represents reactance from the probe feed. At resonance, the input impedance is:

$$Z_{in} = R_{in} + jX_f \tag{2.2}$$

Where X_f is the probe reactance and R_{in} is the total input resistance, composed of the radiation resistance R_{rad}, the conductor loss resistance, the dielectric substrate losses and surface wave losses. For simplicity, the losses are bundled together and antenna input resistance is represented as:

$$Z_{in} = R_{rad} + R_{loss} + jX_f \tag{2.3}$$

From equation 2.3 it becomes clear that for low input impedance, loss resistance starts to dominate the radiation resistance, leading to low radiation efficiency.

2.2. Basic Patch Antenna Design for 96 GHz

To get started, a simple patch antenna was designed that operates at 96 GHz. The design is illustrated in Figure 2.5.

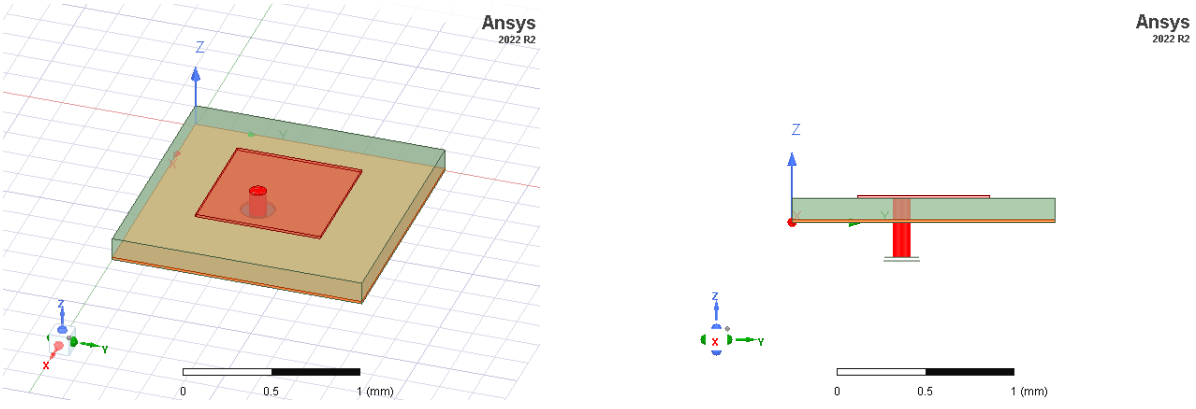

(a) Trimetric view **(b)** Side view

Figure 2.5: 96 GHz probe-fed patch antenna on custom package laminate

Before determining the dimensions of the patch antenna, an initial set of parameters are needed:

- Center frequency f_0: To be able to transmit and receive data for 6G communications, the center frequency should be 96 GHz.
- Substrate dielectric permittivity ϵ_r: The substrate is a custom package laminate. The permittivity is 3.35, with a loss tangent of 0.0055. These specs are supplied by NXP Semiconductors, and are measured at 10 GHz.
- Substrate height is to be chosen up front in the design. To achieve larger bandwidth and high radiation efficiency, a thick substrate of 0.14 mm ($0.047\lambda_0$) was chosen.

Initial dimensions of the patch antenna are based on the basic patch antenna design equations.

The size of the patch dictates the resonant frequency of the antenna. The fields around the patch fringe outwards to the sides (see Figure 2.1b) and also run partly through the air above the patch. This increases the effective length of the patch and decreases the effective permittivity of the substrate respectively.

First, the width of the patch can be calculated:

$$W = \frac{c}{2f_o\sqrt{\frac{\varepsilon_r+1}{2}}} \tag{2.4}$$

Where c is the speed of light ($3 * 10^8$ m/s). Using the calculated value of W the effective dielectric permittivity is then given by:

$$\varepsilon_{reff} = \frac{\varepsilon_r + 1}{2} + \frac{\varepsilon_r - 1}{2}\left[1 + 12\frac{h}{w}\right]^{1/2} \tag{2.5}$$

Now that the dielectric medium around the patch is more accurately known, the length of the patch for a desired resonant frequency can be determined:

$$L_{eff} = \frac{c}{2f_o\sqrt{\varepsilon_{reff}}} \tag{2.6}$$

Then the contribution to this length due to fringing fields is calculated using:

$$\Delta L = 0.412h\frac{(\varepsilon_{reff} + 0.3)\left(\frac{W}{h} + 0.264\right)}{(\varepsilon_{reff} - 0.258)\left(\frac{W}{h} + 0.8\right)} \tag{2.7}$$

Because this fringing effect happens at both ends of the patch, the length extension is subtracted twice from the effective length to get the physical length of the patch:

$$L = Leff - 2\Delta L \tag{2.8}$$

Because the design will have to be used as a dual linear polarized antenna, the patch is made square ($W = L$). Using the equations above, the initial patch design will not create square dimensions thus it was only used as an initial estimate. The exact dimensions of the patch were obtained iteratively using HFSS and are given in Table 2.1.

Table 2.1: Dimensions of square probe-fed patch antenna

Patch Antenna Parameters

f_0	Center Frequency	96 GHz
ϵ_r	Substrate Dielectric Permittivity	3.35
h	Substrate Thickness	0.14 mm
$W = L$	Patch Length and Width	0.75 mm
D_{probe}	Diameter of Probe Feed	0.10 mm
D_{ground}	Diamater of Ground Hole	0.20 mm
y_0	Inset Feed Position	0.25 mm
t_m	Microstrip Metal Thickness	15 µm
$W_s = L_s$	Substrate Length and Width	1.5 mm

The feeding probe was chosen to be thick with a diameter of 0.10 mm. This reduces probe reactance and provides a physically stronger shape for fabrication. The hole in the ground is chosen to be 20 mm to accommodate a good clearance between the probe and the ground plane. The hole is slightly smaller than a piece of 50 Ω air-filled coaxial line which has a shield diameter of 0.23 mm, creating a ring-shaped coupling slot. This slot can partially compensate for feeding probe reactance [17]. Because the feeding network is not within the scope of this thesis, the piece of coaxial line has been de-embedded from the simulation results. The inset feed position was tuned to match 50 Ω and the unit cell was designed to be 1.5 mm or half-wavelength at 100 GHz to prevent grating lobes when used in an array. The microstrip metal thickness determines the thickness of the ground plane and patch. A thickness of 15 µm is in agreement with NXP's AiP technology specifications.

2.2.1. Input Impedance and Bandwidth

The antenna design has been simulated over a range of frequencies using a 50 Ω wave-port excitation. The input impedance is plotted in Figure 2.6.

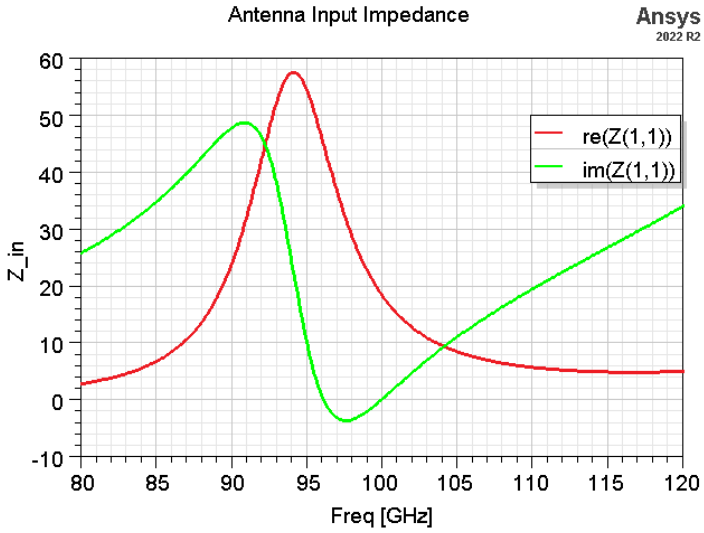

Figure 2.6: Input impedance of patch antenna

As can be seen from Figure 2.6, the antenna resonates around 94 GHz, however due to probe reactance, the input impedance contains a large inductance at this frequency. The impedance should be purely real at the desired frequency and this is achieved as can be seen from the green curve crossing the 0 Ω point at 96 GHz.

The real part of the impedance, shown in red, is around 50 Ω at 96 GHz, indicating a good match at the antenna port. If the antenna impedance changes with respect to the port impedance, reflections of the incident voltage at the port occur, and less power reaches the antenna. The reflection coefficient, also known as S_{11} is given by:

$$\Gamma = \frac{Z_L - Z_0}{Z_L + Z_0} \tag{2.9}$$

The signal enters the antenna without reflections when $Z_L = Z_0$. The reflection coefficient then equals zero. A common way to show the reflective behaviour of the antenna is the antenna's return loss. The return loss in dB is calculated from the reflection coefficient using:

$$RL = 20 * log_{10}|\Gamma| \tag{2.10}$$

The return loss of the patch antenna is given in Figure 2.7. The antenna is very well matched at 96 GHz but has a narrow-band response. The bandwidth of the antenna is often defined as the frequency

range between the -10 dB points of the return loss. For this antenna, the -10 dB bandwidth equals 5.2 GHz (93.3 - 98.5 GHz) or 5.1%.

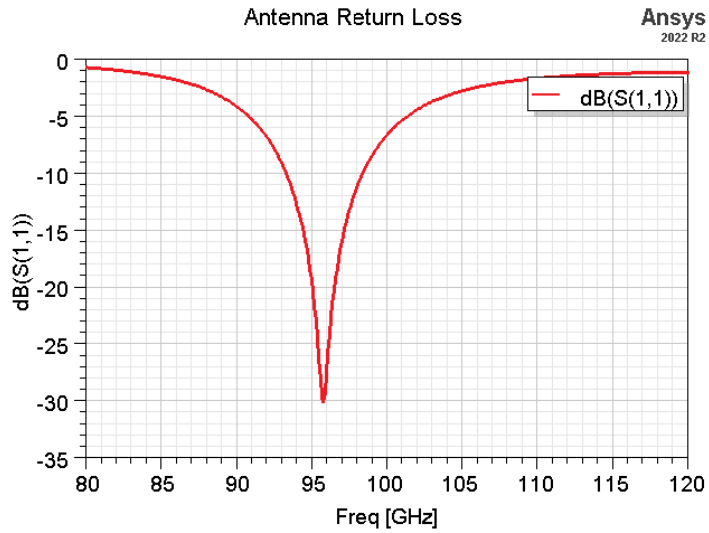

Figure 2.7: Input return loss of patch antenna for a 50 Ω port

With an initial patch antenna design, the bandwidth is clearly too low for the desired spec of 20%. A bandwidth widening technique has to be applied to extend the bandwidth.

2.3. 50 Ω Dual-Polarized Stacked Patch Antenna

A variety of broadbanding techniques exist for patch antennas. A common way to increase bandwidth is to widen the patch. This lowers the antenna Q-factor by increasing the volume below the patch. Because the antenna design requires dual polarization, the antenna design along the x-axis needs to be identical to the design along the y-axis. For this reason the patch has to be square and cannot be made wider. Alternatively, the substrate can be made thicker, but this increases probe reactance and introduces more radiation from the probe and surface waves.

A far better solution is to introduce an additional resonance. By adding an extra layer of substrate, fitted with a passive patch, on top of the design, a dual resonance antenna is created. Such a configuration is called a stacked patch antenna and was first introduced in [18]. If both resonances are close to each other and have a low quality factor, the bandwidth of one resonance transitions smoothly into the other resonance, creating an overall large bandwidth. A design approach for stacked patch antennas with bandwidth in excess of 25% is given in [19].

Similar to how a single patch antenna can be model as a RLC resonator, a stacked patch antenna can be modelled as two RLC resonators, coupled by a transformer. The equivalent circuit of a probe-fed stacked patch antenna is given in Figure 2.8. Coupling factor k_1 can be set to 1 and the coupling factor k_2 can be tuned iteratively to match the electromagnetic coupling behaviour of the stacked patch. Although this circuit can mimic the impedance behaviour versus frequency, it is very hard to correlate values of the lumped components to physical parameters of the antenna.

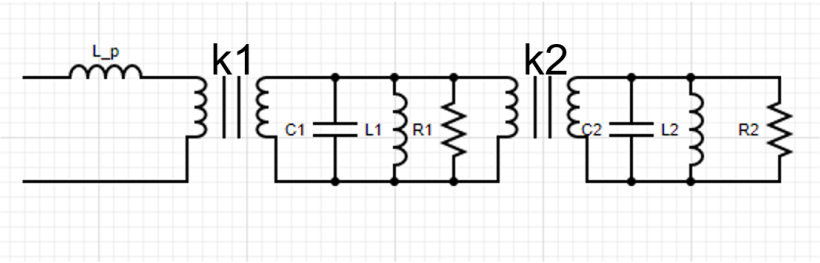

Figure 2.8: Equivalent circuit of a probe-fed stacked patch antenna

A 50 Ω reference stacked patch antenna was designed using methods from [19] as a guide and is shown in Figure 2.9. The antenna is fitted with an extra feed to make it dual linearly polarized. The antenna behaves identically for both x- and y polarization because patches are square and the feeds are positioned at equal inset distances from the edge. The passive, or parasitic patch is placed above the active patch on a thick dielectric layer. Both dielectric layers use the same package laminate substrate with a permittivity 3.35.

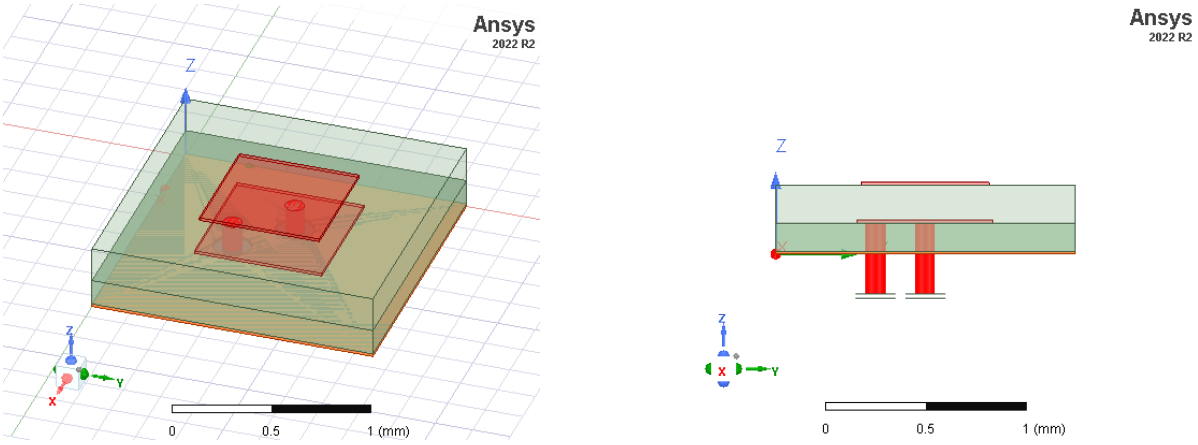

(a) Trimetric view **(b)** Side view

Figure 2.9: 96 GHz dual-polarized probe-fed stacked patch antenna on custom package laminate

The dimensions of the stacked patch antenna design are given in Table 2.2.

Table 2.2: Dimensions of 50 Ω dual-polarized probe-fed stacked patch antenna

Patch Antenna Parameters		
f_0	Center Frequency	96 GHz
ϵ_r	Substrate Dielectric Permittivity	3.35
h_1	Bottom Substrate Thickness	0.14 mm
h_2	Top Substrate Thickness	0.19 mm
$W_1 = L_1$	Active Patch Length and Width	0.68 mm
$W_2 = L_2$	Passive Patch Length and Width	0.64 mm
D_{probe}	Diameter of Probe Feed	0.10 mm
D_{ground}	Diameter of Ground Hole	0.20 mm
y_0	Inset Feed Position	0.09 mm
t_m	Microstrip Metal Thickness	15 µm
$W_s = L_s$	Substrate Length and Width	1.5 mm

R. B. Waterhouse (2000) in [19] gives a starting point for a stacked patch design by making the passive

patch size equal to the active patch and make the upper substrate layer 1.5x the thickness of the lower substrate layer. A problem with this strategy is that the paper uses a low permittivity substrate at the bottom ($\epsilon_r = 2.2$) and foam as the top substrate ($\epsilon_r = 1.07$) whereas the design in this work is limited to only use the package laminate ($\epsilon_r = 3.35$). The dimensions in Table 2.2 were acquired using iterative simulations. Despite this, impedance tuning strategies from the paper still apply and were used to match the antenna to the port impedance.

2.3.1. Input Impedance and Bandwidth

Simulations reveal the input impedance for the stacked patch antenna, given in Figure 2.10. Because the patches are square and the feeds are positioned with the same inset distance, impedance is the same for both polarizations. As can be seen from Figure 2.10, the dual resonance allows a large range of frequencies to have 50 Ω input resistance with near zero reactance.

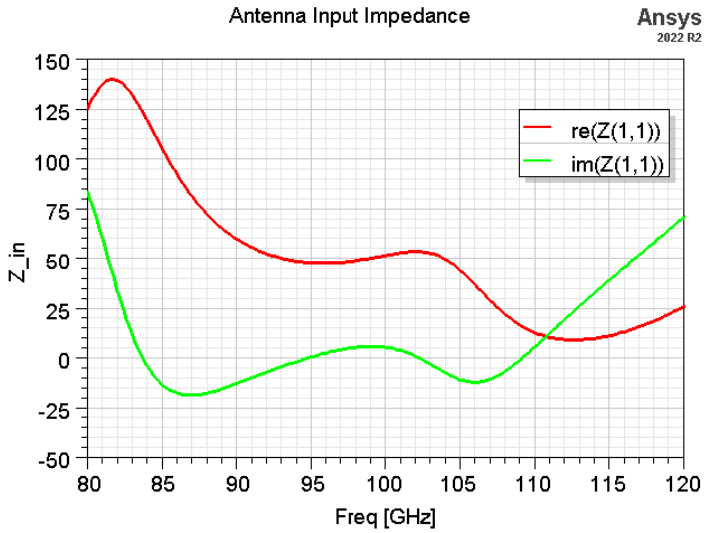

Figure 2.10: Input impedance of stacked patch antenna

Matching of the antenna to a 50 Ω port is shown as return loss in Figure 2.11. The -10 dB bandwidth can be derived from this graph and is 21.2 GHz (86.0 - 107.2 GHz) or 22.1%, meeting the bandwidth design goal of this work.

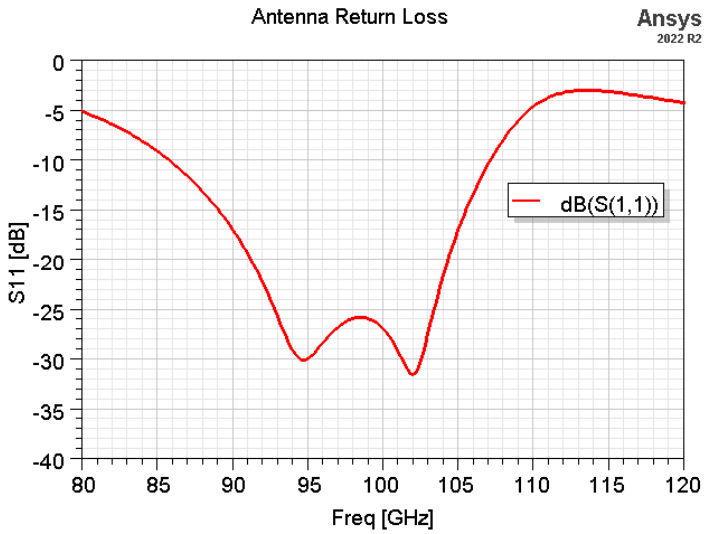

Figure 2.11: Return loss of stacked patch antenna for a 50 Ω port

To tune the antenna, the Smith chart was used to visualize impedance as a function of frequency. When the passive patch is added to the design, the dual resonance shows on the Smith chart as a knot in the impedance locus, see Figure 2.12. To have a well matched antenna, this knot should be centered on the Smith chart, where Γ approaches zero. The figure shows a black arc indicating the change in position of the locus knot with changing size of the passive patch. When the passive patch is made bigger, the knot moves to the right, when it is made smaller, it moves to the left. The blue arc shows variation of the knot position with changing feed position, although this variation is less sensitive. Moving the feed towards the patch edge moves the knot up on the Smith chart, placing the feed more towards the patch's center moves the knot down. Using these dependencies the antenna was tuned.

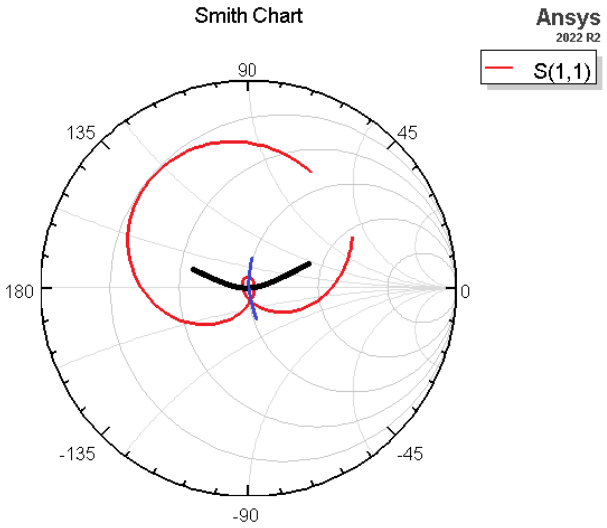

Figure 2.12: Input impedance of stacked patch antenna on 50 Ω Smith chart

2.3.2. Port Coupling

It is important that coupling between the antenna ports is kept as low as possible to prevent power from one port leaking into the other, effectively lowering the radiated power. An effective way to visualise the amount is coupling is by considering the dual-polarized antenna as a two-port system. The transmission coefficient or S_{21} represents how much of the incident amplitude is seen at the output port. From the transmission coefficient the insertion loss can be calculated, representing the port coupling:

$$IL = -20 * log_{10}|S_{21}| \tag{2.11}$$

Ideally, the port coupling equals -∞, meaning that from the power entering one port, none exits through the other. This ensures both polarizations of the antenna can be used simultaneously and independently. The port coupling of the stacked patch antenna is given in Figure 2.13. The amount of coupling is below -20 dB along the full bandwidth which is an acceptable amount.

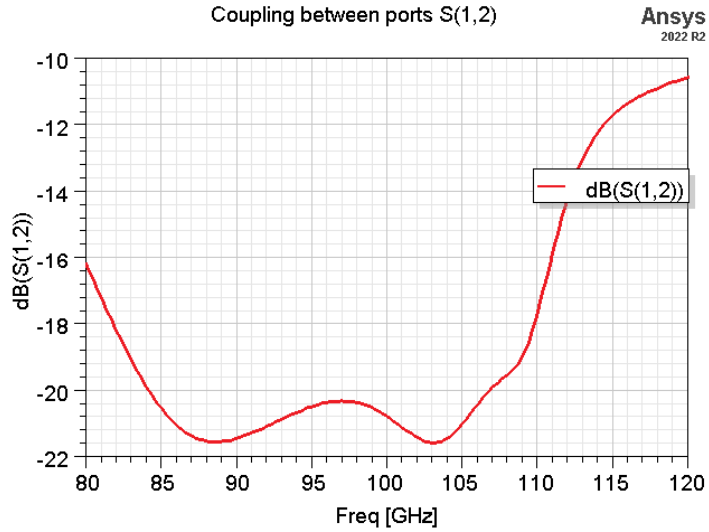

Figure 2.13: Insertion loss of dual-polarized stacked patch antenna, indication coupling between the two ports

2.3.3. Radiation Performance

Antenna radiation was simulated by exciting the Y-polarized port. The X-polarized port was connected to a matched load. HFSS simulations at 92, 96 and 100 GHz report a radiation efficiency of 96.1%, 96.1% and 95.5% respectively. The efficiency is likely to be higher than what is realistically achievable using the package laminate technology. The radiation efficiency is mostly dependent on losses in the antenna, which require metrics at the frequency of operation to accurately model. The loss tangent of 0.0055 that is used in the simulations is measured at 10 GHz but is assumed to be higher at 96 GHz. Because there is no data on the laminate at this frequency, the dielectric losses are not accurately modeled. Additionally, surface roughness of the conductors increases conductor losses, lowering radiation efficiency. Again due to lack of data, surface roughness was not included in the model. Despite this, geometry also plays a role in the radiation efficiency and a relative comparison between efficiencies is still valid to assess the design.

The radiation patterns in E-plane and H-plane are given in Figure 2.14. The co-polarized gain is maximum at broadside with 6.04 dB and shows an asymmetrical back-lobe due to the antenna feed. Cross-polarization levels are below -20 dB with respect to the co-polarized gain in E-plane. In H-plane there is a peak of -16 dB with respect to the co-polarized gain at $\theta = -30°$ due to the X-polarized feed (passive in this simulation).

The antenna is required to provide a consistent radiation pattern over the operational bandwidth. To illustrate this, the co-polarized gain is plotted in both E-plane and H-plane for 92, 96 and 100 GHz in Figure 2.15. In H-plane, the antenna provides a very consistent radiation pattern that is independent of frequency. In E-plane, there is a slight reduction in gain for higher frequencies around $\theta = -40°$ due to the feeding probe. The difference in gain between 92 and 100 GHz at this angle is around 0.5 dB which is acceptable.

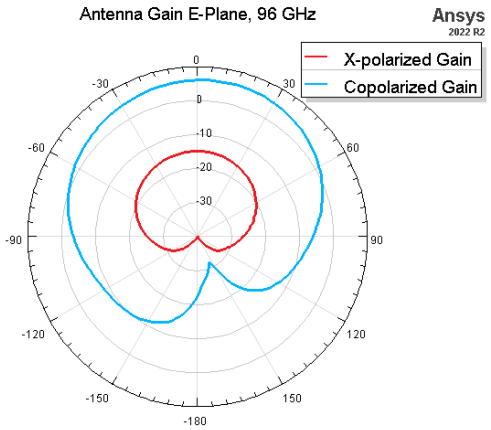

(a) Radiation pattern in E-plane cut

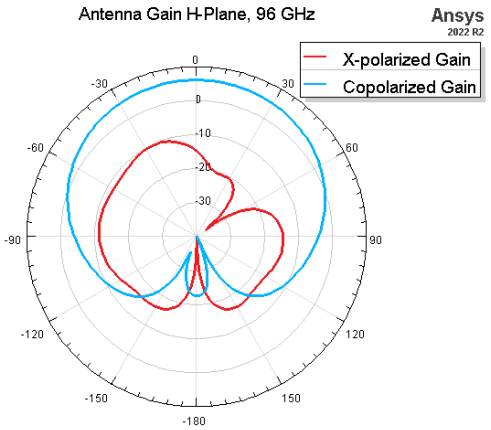

(b) Radiation pattern in H-plane cut

Figure 2.14: 96 GHz cross- and co-polarized radiation patterns

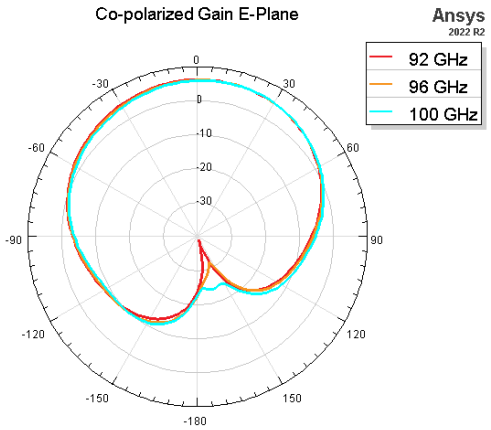

(a) Co-polarized radiation pattern vs. frequency in E-plane cut

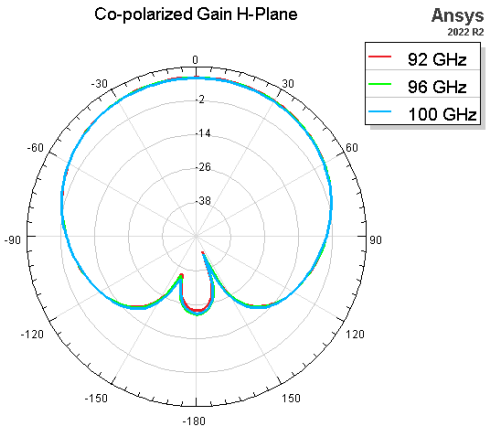

(b) Co-polarized radiation pattern vs. frequency in H-plane cut

Figure 2.15: Co-polarized radiation patterns at 92, 96 and 100 GHz

The stacked patch configuration is suitable for large bandwidth antenna array elements. Now that the benchmark has been set with a 50 Ω design, using tuning methods such as varying patch size and feed position a 25 Ω design is feasible. The following section provides a detailed description on this design, the challenge of probe reactance and proposed solutions.

2.4. 25 Ω Dual-Polarized Stacked Patch Antenna

For the initial design of a 25 Ω antenna, the same principles from the 50 Ω reference design were used. The feeds were moved more towards the center of the patch to lower the input resistance. Additionally, the upper patch was made smaller w.r.t the bottom patch to further reduce resistance at the higher resonance, and both patches were scaled to adjust for frequency shifts. The design parameters are given in Table 2.3.

Table 2.3: Dimensions of 25 Ω dual-polarized probe-fed stacked patch antenna

Patch Antenna Parameters		
f_0	Center Frequency	96 GHz
ϵ_r	Substrate Dielectric Permittivity	3.35
h_1	Bottom Substrate Thickness	0.14 mm
h_2	Top Substrate Thickness	0.19 mm
$W_1 = L_1$	Active Patch Length and Width	0.73 mm
$W_2 = L_2$	Passive Patch Length and Width	0.64 mm
D_{probe}	Diameter of Probe Feed	0.10 mm
D_{ground}	Diameter of Ground Hole	0.20 mm
y_0	Inset Feed Position	0.14 mm
t_m	Microstrip Metal Thickness	15 µm
$W_s = L_s$	Substrate Length and Width	1.5 mm

2.4.1. Input Impedance and Bandwidth

The input impedance as a function of frequency is given in Figure 2.18a. Although the input resistance is close to 25 Ω over the desired bandwidth, there is a significant amount of probe reactance that cannot be eliminated by tuning methods from [19]. The reactance is causing a mismatch at the 25 Ω antenna port, leading to larger voltage reflections compared to the 50 Ω reference. Figure 2.18b shows the return loss of the antenna and is clearly worse in terms of matching compared to the 50 Ω antenna in Figure 2.7. On a 25 Ω Smith chart, see Figure 2.17, it becomes even more obvious, as the locus knot of the antenna impedance is not centered.

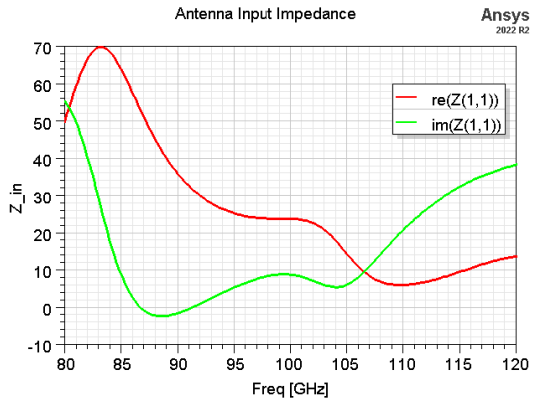

(a) Input Impedance of 25 Ω antenna element

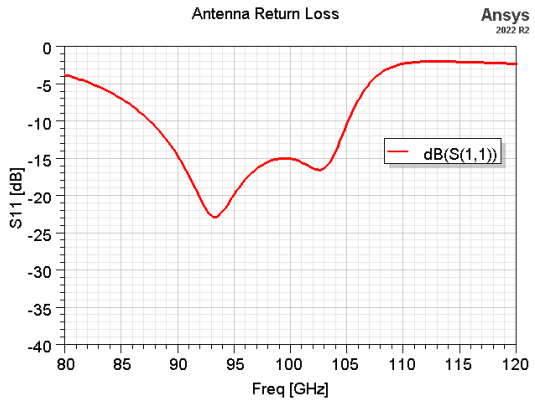

(b) Return loss of 25 Ω antenna element

Figure 2.16: 25 Ω dual-polarized stacked patch antenna impedance and return loss

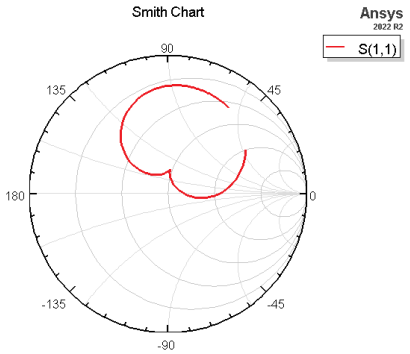

Figure 2.17: Impedance of the antenna on a 25 Ω Smith chart

Several options were explored to compensate for the reactance in the antenna impedance. In a first attempt, the hole in the ground plane where the feed runs through was made smaller to create capacitance to ground [17], see Figure 2.19. The reactance was reduced by 2j Ω, even when the gap between the ground plane and the feeding probe was only 15 microns. Taking fabrication tolerances into consideration, there is a significant risk of shorting the signal probe to ground due to a fabrication error. Thus this solution was not deemed to be feasible.

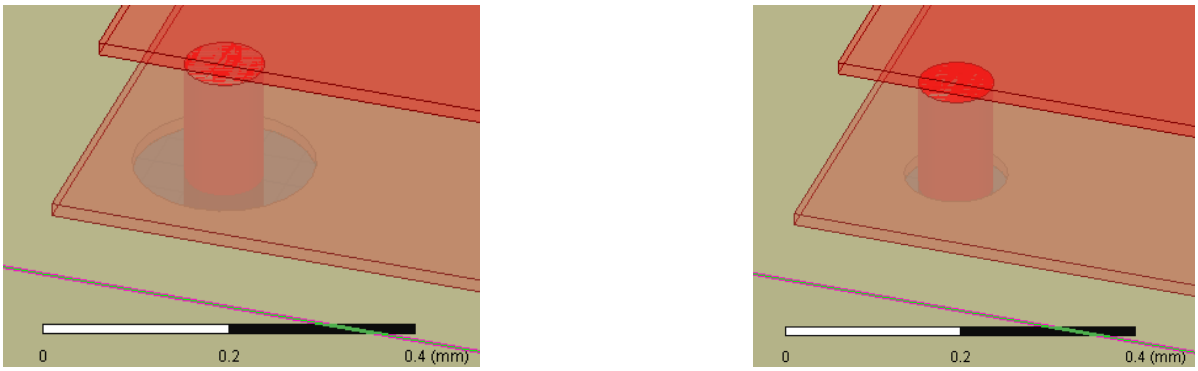

(a) Normal clearance between ground plane and feed

(b) Small clearance to create capacitive ring

Figure 2.18: Probe inductance compensation using capacitive ring at ground plane interface

Alternatively, a series capacitance can be added at the feeding probe. The part of the patch where the probe feed connects can be capacatively coupled to the rest of the patch by cutting a square slot at the feed location [20]. This method was applied on the dual-polarized stacked patch design, shown in Figure 2.19a. Both feeding probes terminate into a small patch, which then couples to the patch antenna using capacitance. The upper patch is not visible in this figure.

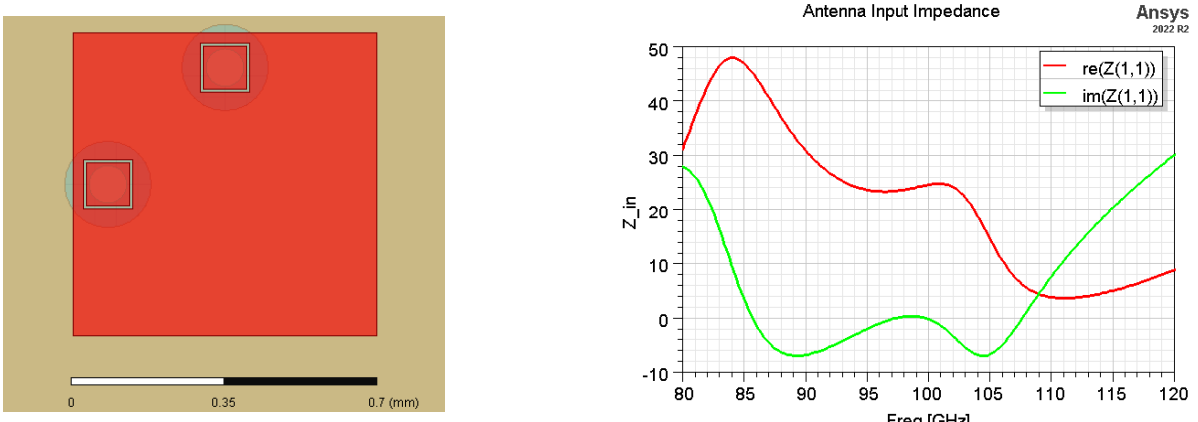

(a) Top view of the active patch, showing capacitive feeding using square slots

(b) Input impedance

Figure 2.19: Capacitive fed stacked patch antenna

The probe reactance can be accounted for using a gap of 14 microns between the feeding patch and the antenna patch. The resulting antenna impedance is given in Figure 2.19b. The antenna is well matched to a real 25 Ω port at the center frequency of 96 GHz. A drawback is that the impedance tuning is very sensitive to the width of the gap. Again, taking fabrication tolerances into account, the inevitable variance in the width of the gap becomes a problem and this design is not feasible.

Lastly, by reducing the height of the bottom substrate layer, the feeding probe is shortened and probe reactance is reduced. This is by far the most effective method to tune the antenna to a real load however it can come at the expense of lower radiation efficiency and bandwidth. For the antenna design depicted in Table 2.3, the bottom substrate height was reduced from 0.14 mm to 0.12 mm, and additional fine

tuning was done to both patches. The impedance became matched at 25 Ω, as can be seen in Figure 2.20 where the locus of the impedance is properly centered on the Smith chart.

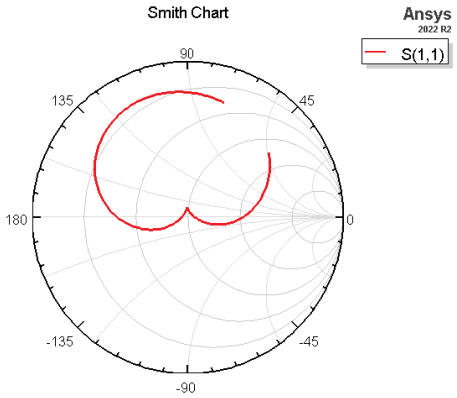

Figure 2.20: Impedance of antenna with reduced bottom substrate height on a 25 Ω Smith chart

2.4.2. Cavity-Backed Antenna

Patch antennas can be backed by a cavity by placing electric walls around the patch. In AiP technology, these walls are made of copper vias, connecting a strip at the top layer to the ground plane. This principal is shown in Figure 2.21. The copper strip connected to the top of the vias is fabricated on the same metal layer as the passive patch. The vias are the same diameter as the feeding probes and are spaced closely together such that the gap between vias is less than $\lambda/20$.

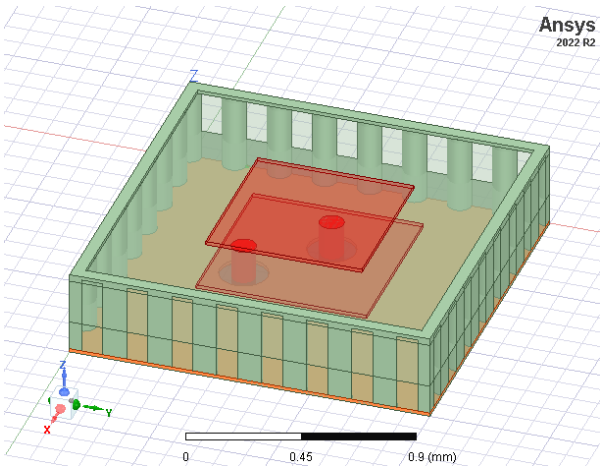

Figure 2.21: Trimetric view of cavity-backed stacked patch antenna

Cavity backing of patch antennas is typically done to reduce the propagation of surface waves [21]. In addition, they can also provide higher gain, bandwidth and radiation efficiency for patch antennas [22]. A study on cavity-backed patch antennas for phased arrays has found a reduction in energy transfer between antenna elements due to the cavities acting as isolation structures [23].

Since the goal of this thesis is to design a 8x8 phased array antenna, cavity backing was investigated in this work. It was found that by loading the antenna with a cavity, it was still possible to tune the antenna as a 25 Ω resistive load without significant reactance. In this study, the cavity was modelled as a solid copper wall instead of a wall of vias. This was done to reduce the complexity of the geometry, thereby reducing the amount of tetrahedrons required to form the mesh for finite-element method solvers in HFSS and ADS, significantly simulation time and memory usage. The design of a 25 Ω cavity-backed stacked patch antenna is shown in Figure 2.22 and design parameters are detailed in Table 2.4. Probe reactance was reduced by reducing the bottom substrate height, shortening the probe.

Table 2.4: Dimensions of 25 Ω cavity-backed dual-polarized probe-fed stacked patch antenna

Patch Antenna Parameters

f_0	Center Frequency	96 GHz
ϵ_r	Substrate Dielectric Permittivity	3.35
h_1	Bottom Substrate Thickness	0.125 mm
h_2	Top Substrate Thickness	0.19 mm
$W_1 = L_1$	Active Patch Length and Width	0.76 mm
$W_2 = L_2$	Passive Patch Length and Width	0.64 mm
D_{probe}	Diameter of Probe Feed	0.10 mm
D_{ground}	Diameter of Ground Hole	0.20 mm
y_0	Inset Feed Position	0.05 mm
t_m	Microstrip Metal Thickness	15 µm
$W_s = L_s$	Substrate Length and Width	1.5 mm

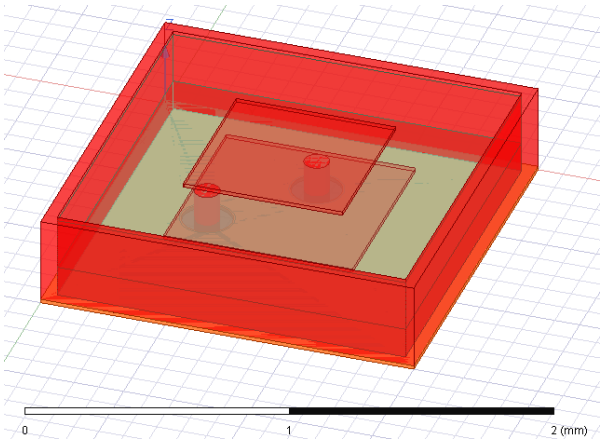

Figure 2.22: Trimetric view of simplified cavity-backed stacked patch antenna for use in arrays

Impedance results for this antenna are shown in Figure 2.23 on a 25 Ω Smith chart (a) and as the return loss for a 25 Ω port (b). The bandwidth is 15 GHz (89 - 104 GHz) or 15.6%.

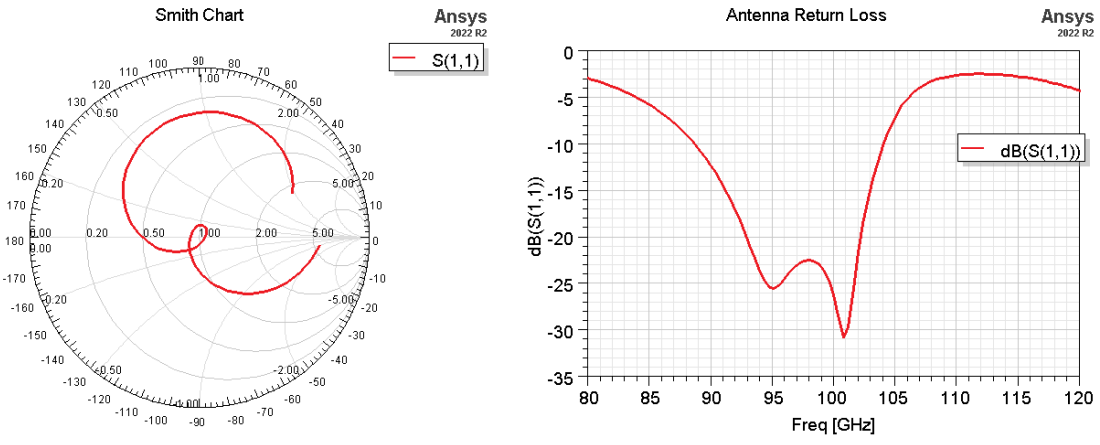

(a) 25 Ω Smith chart

(b) Return loss

Figure 2.23: Impedance results for simplified cavity-backed stacked patch antenna

2.4.3. Radiation Performance

Similar to the 50 Ω reference antenna, the cavity-backed antenna was simulated at 92, 96 and 100 GHz to evaluate the radiation. The radiation efficiency at these frequencies was found to be 94.2%, 94.2% and 91.8% respectively. From this we can conclude that despite the cavity-backed design promising higher radiation efficiency according to [22], it is still lower than the 50 Ω reference. Most likely this difference is caused by the lower input resistance, causing the loss resistance to become more significant w.r.t. the radiation resistance, see equation 2.3. The radiation patterns are given in Figure 2.24 and Figure 2.25. The co-polarized gain is maximum at broadside at 5.67 dB, which is about 0.4 dB less than the 50 Ω reference. Additionally the cross-polarized gain in Figure 2.24a peaks at around -15.7 dB with respect to the co-polarized gain. This is higher than the 50 Ω reference and is also above the desired spec -20 dB. In Figure 2.24b the cross-polarized gain maximises at an angle around $\theta = -30°$ similar to the reference antenna, however the difference between the co-polarized gain at this angle is -12 dB compared to -16 dB difference for the 50 Ω reference antenna.

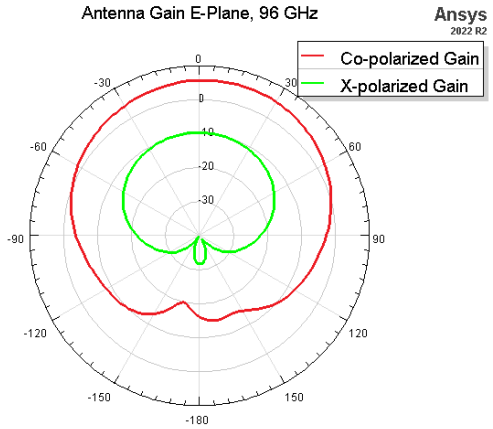

(a) Radiation pattern in E-plane cut

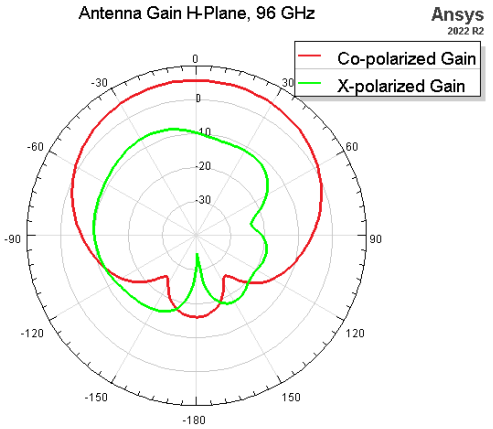

(b) Radiation pattern in H-plane cut

Figure 2.24: 96 GHz cross- and co-polarized radiation patterns

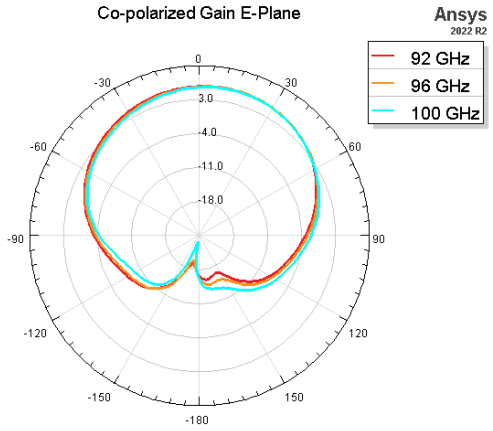

(a) Co-polarized radiation pattern vs. frequency in E-plane cut

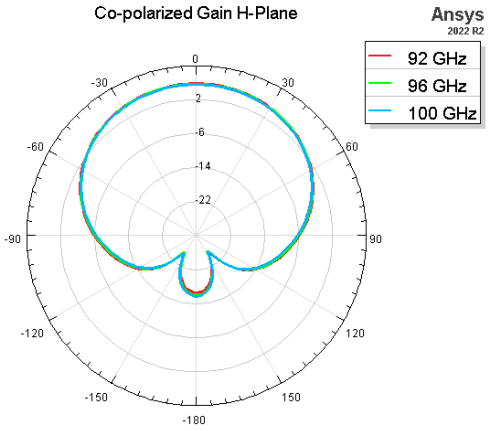

(b) Co-polarized radiation pattern vs. frequency in H-plane cut

Figure 2.25: Co-polarized radiation patterns at 92, 96 and 100 GHz

2.5. Conclusions

In this chapter, the microstrip patch antenna has been introduced. The coaxial probe feed was explained and its effects on the antenna input impedance has been explained using an equivalent circuit model. An initial design was made for 96 GHz using a basic patch antenna, from which it was determined that broadbanding techniques were needed to meet the bandwidth requirement. From this, the

stacked patch antenna was introduced. A 50 Ω reference design was made, along with a 25 Ω design for direct impedance matching to the power amplifier. As has been explained in the introduction, a trade-off is expected when it comes to tuning an antenna to a low impedance. Although a 25 Ω antenna design was achieved, compared to the 50 Ω design it had:

- Lower bandwidth, 15.6% compared to 22.1%.
- Lower radiation efficiency, 94.2% compared to 96.1% at the center frequency.
- Lower gain, 5.76 dB compared to 6.04 dB.
- 4 dB higher level of cross-polarization.

A more complete comparison is done in the next chapter, where the antenna designs are used as elements of an 8x8 array.

3

Beamforming: 8x8 Phased Array

In this chapter, the design of 8x8 planar phased arrays is given based on the antenna unit cell designs from Chapter 2. First, the concept of phased arrays is explained. Then the reference and novel array designs are presented. To conclude this chapter, the performance of both designs are assessed and a comparison is made.

3.1. Background Information

As has been mentioned in the introduction of this thesis, antenna arrays provide the benefit of high gain antenna radiation because of a larger aperture. This relation is shown in formula 3.1 and follows from the ratio between the antenna effective aperture (A_e) and the aperture of an isotropic unity gain antenna.

$$G = \frac{4\pi A_e}{\lambda^2} \tag{3.1}$$

By combining antennas together into an array of size $N \times N$ the gain increases proportionally by factor N^2. This happens because the effective aperture increases due to coherent in-phase adding of the signal from array elements. For an 8x8 array, there are 64 elements and thus the gain increases by a factor of 64, or 18 dB. This very high directivity of the antenna helps to overcome the burden of a small physical aperture at these short wavelengths. As the name suggests, high directivity implies that the radiation is focused into a beam. With equal phase and uniform excitation of the array elements, this beam is aimed in the broadside direction and the half-power beam width (HPBW) is inversely proportional to the directivity. To establish a communication link, antenna alignment is crucial because the antenna gain outside of the main beam is very low. This is where phased arrays provide the solution. By introducing a progressive phase shift on the excitation of antenna elements in the array, the direction along which the radiation is constructively added can be steered. For regular planar arrays of size $N \times N$, the degrees of phase shift on element E_{ij} where $i, j = 1, 2, ..., N$ is given by:

$$\Phi_{ij} = \beta_x * (i-1) + \beta_y * (j-1) \tag{3.2}$$

Where β_x and β_y are the progressive phase shifts in the x and y direction in degrees, and are calculated for a desired beam-steering angle (θ, ϕ) using:

$$\beta_x = \frac{-180}{\pi} k d_x sin(\theta) cos(\phi) \tag{3.3}$$

$$\beta_y = \frac{-180}{\pi} k d_y sin(\theta) sin(\phi) \tag{3.4}$$

Where k is the wavenumber, d_x and d_y is the element spacing in the x and y direction respectively and θ and ϕ are the steering angles in elevation and azimuth respectively, with $\theta = 0^\circ$ being the broadside direction. Because the elements are square with sides of 1.5 mm, $d_x = d_y = 1.5 * 10^{-3}$.

3.2. Dual-Polarized Stacked Patch Antenna Array

Using the antenna element designs from Chapter 2 as a basis, antenna arrays of size 8x8 are designed. The arrays were designed iteratively using tuning methods from [19]. Both the reference array of 50 Ω and the direct impedance matched array of 25 Ω follow the same design principal using a probe fed stacked patch with cavity backed elements. This ensures a fair comparison between the arrays, with the sole difference being the impedance. Cavity backed elements were chosen to provide a more stable impedance when scanning the beam, which is key in providing an efficient power delivery at the PA output. This effect is shown in appendix A, where a full comparison is done between two 50 Ω antenna arrays, one with cavity backed elements and one without cavities.

Figure 3.1 shows a top view of both designs. Both arrays measure exactly 12 mm in length and width with a total height of 0.365 mm. Cavity walls 0.10 mm wide are fitted around each element and the perimeter of both arrays. In Figure 3.1b labels are added to a selection of elements that are used in this chapter to compare impedance and port coupling.

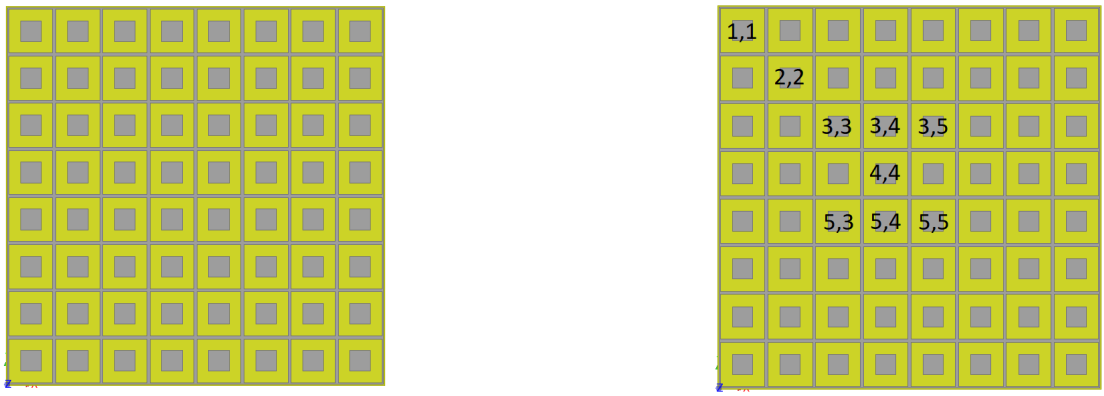

(a) 50 Ω reference design

(b) 25 Ω direct impedance matched design

Figure 3.1: Top view of 8x8 antenna array

Dimensions of the arrays are given in Table 3.1. Most design parameters are the same between both designs. Both designs feature thick feeding probes and a thinner bottom substrate layer to reduce probe reactance. Patch sizes are tuned for both designs to match the antenna to a 50 Ω and 25 Ω impedance around the center frequency using the same methods used in Chapter 2.

Table 3.1: Dimensions of both antenna array designs

Patch Antenna Parameters		50 Ω design	25 Ω design
f_0	Center Frequency	96 GHz	96 GHz
ϵ_r	Substrate Dielectric Permittivity	3.35	3.35
h_1	Bottom Substrate Thickness	0.125 mm	0.125 mm
h_2	Top Substrate Thickness	0.21 mm	0.21 mm
$W_1 = L_1$	Active Patch Length and Width	0.70 mm	0.74 mm
$W_2 = L_2$	Passive Patch Length and Width	0.66 mm	0.65 mm
D_{probe}	Diameter of Probe Feed	0.10 mm	0.10 mm
D_{ground}	Diameter of Ground Hole	0.20 mm	0.20 mm
y_0	Inset Feed Position	0.09 mm	0.09 mm
t_m	Microstrip Metal Thickness	15 µm	15 µm
$W_s = L_s$	Substrate Length and Width	12 mm	12 mm

3.2.1. Simulation Approach

It can be noted that the dimensions of the antenna array differ from the dimension of the antenna elements. Because mutual coupling and mutual impedance play a large role in the design of antenna arrays, simply taking a unit cell design and placing it into an array will not have the desired performance. The antenna needs to be re-tuned by varying patch sizes, feed position and substrate height. This is particularly challenging as this is an iterative optimization process, and computational analysis of the design using EM-solvers takes several hours for arrays of this size.

An alternative method to designing the array is to simulate the antenna element using periodic boundaries at the sides, allowing the simulation of an infinitely large array. This analysis shows the impedance and radiation of the antenna as an embedded element with infinitely many neighbouring elements. This type of simulation is much faster but is only representative for center elements in very large arrays ($N > 20$). Mutual coupling effects are very different for edge and corner elements, as they are only affected by coupling from neighbours in certain directions. Infinite array simulations do not take these edge effects into account.

This leaves no other option than a full finite array simulation for accurate results. Despite this, there are still ways to reduce simulation time. The most important factor is computational resources. By using many cores, multiple frequencies can be computed in parallel. Additionally, domain decomposition method (DDM) can be used. This method exploits the fact that the array is comprised of a single element design. A mesh is only generated for one element and then copied to all the other elements in the array. The array is then split up into domains and using boundary conditions, continuity of the electromagnetic fields is enforced. This significantly reduces meshing time and speeds up EM-solving by allowing the domains and frequencies to be solved in parallel.

For the design of the antenna arrays in this work, HFSS was used using FEM with DDM enabled. Using HPC resources, 24 cores were used with a reservation of 120 GB of memory. HFSS uses adaptive meshing, a method that iteratively refines the mesh until it converges on an accurate representation of the design. Each adaptive pass is compared with the last iteration and the S-parameters are compared. The difference between each pass is the ΔS parameter, which was set to a threshold of 0.01 to finish the meshing process.

3.3. Impedance, Bandwidth and Scanning

Input impedance of the antenna array has to be decomposed as the contribution of every element in the array. Center elements will have a different impedance than edge elements, despite having identical element design. Moreover, because of mutual coupling, impedance of elements have to be evaluated when the entire array is excited. The excitation is done with uniform amplitude distribution on the y-polarized feed such that the radiation in the direction of the beam is of maximum power. Input impedance of array elements can then be evaluated under any scanning angle.

3.3.1. Impedance versus Element Position

For both 8x8 array designs, four elements were compared at broadside scanning ($\theta = 0$) to illustrate the effects of load modulation throughout the array. Figure 3.2 shows the return loss of these elements w.r.t. the design impedance. In this case the return loss curves are the active S11 parameters, meaning that all the elements in the array are simultaneously excited.

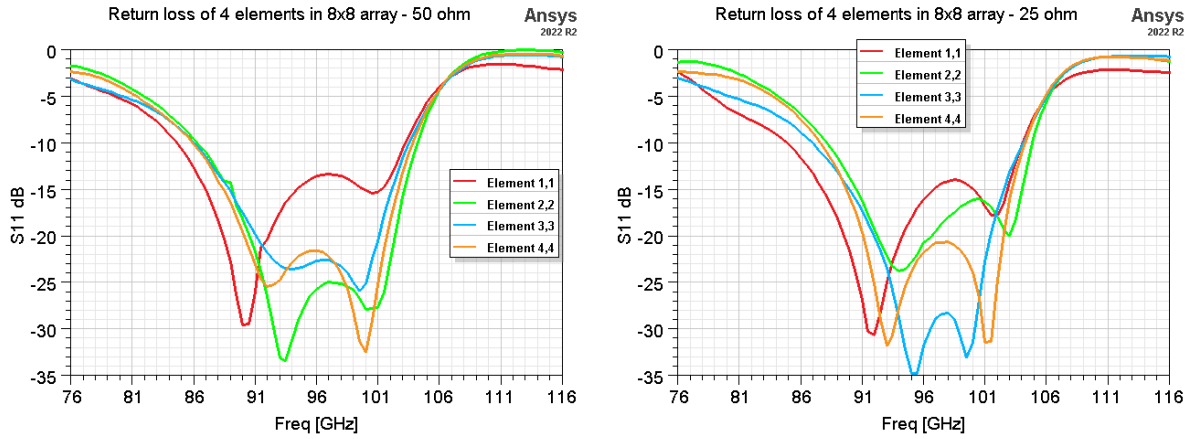

(a) 50 Ω reference design

(b) 25 Ω direct impedance matched design

Figure 3.2: Return loss of four antenna elements in the 8x8 array

The 50 Ω reference array shows the elements are well matched at the center frequency of 96 GHz. Only the corner element is somewhat reflective at the port but it is still below the -10 dB mark. The -10 dB bandwidth of the reference array is between 86 and 103 GHz. The 25 Ω antenna array shows very similar return loss compared to the reference. Again all the elements are well matched at the center frequency. The bandwidth is a slightly more narrow between 88 and 104 GHz. Nevertheless, the bandwidth is well centered around 96 GHz.

3.3.2. Impedance vs Scanning Angle

While the input impedance varies between elements in the array, it also depends on the scanning angle of the beam. Phase shifts in the excitation significantly affect the impedance, especially for large scanning angles. To illustrate this effect, the impedance of a center element (4,4) is plotted on a Smith chart in Figure 3.3 for scanning in H-plane, and in Figure 3.4 for scanning in E-plane.

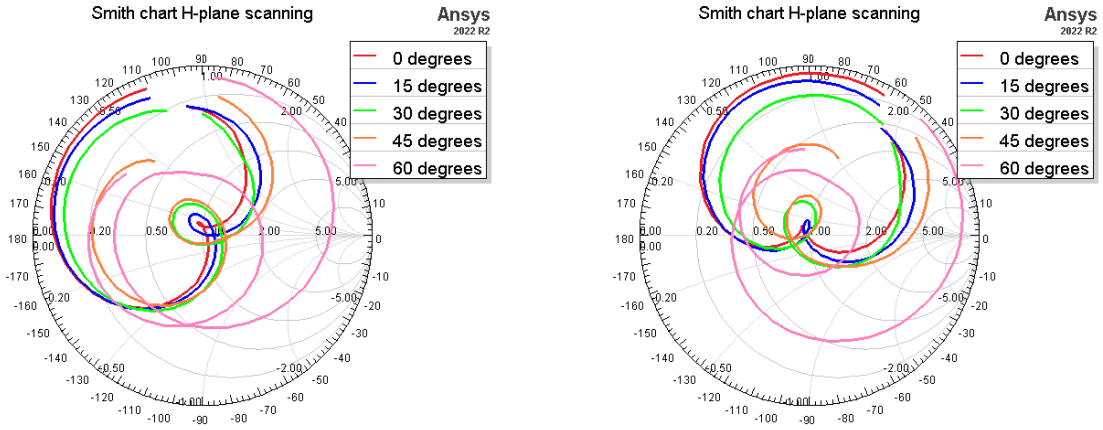

(a) 50 Ω reference design

(b) 25 Ω direct impedance matched design

Figure 3.3: Impedance of element (4,4) vs scanning angles $0°$ to $60°$ in H-plane

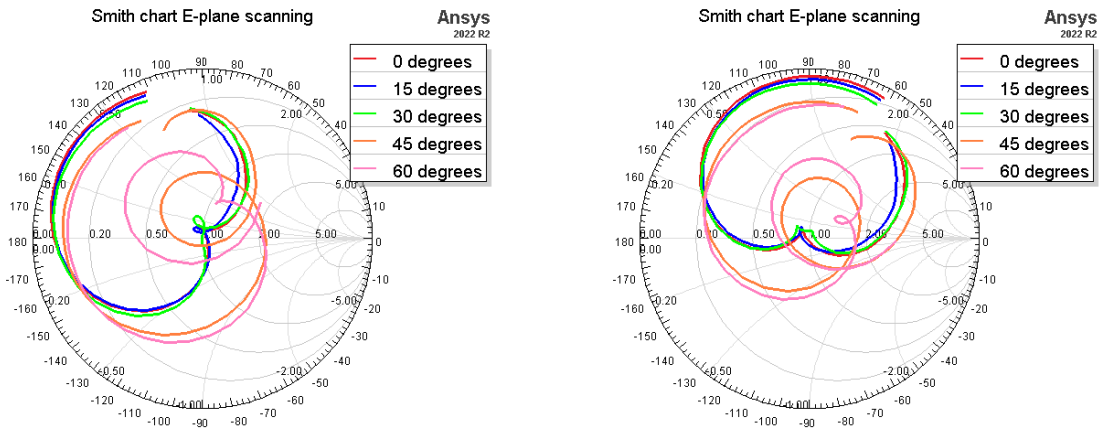

(a) 50 Ω reference design

(b) 25 Ω direct impedance matched design

Figure 3.4: Impedance of element (4,4) vs scanning angles 0° to 60° in E-plane

The loop in the locus on the Smith chart increases in size for larger scanning angles. This indicates the dual resonance of the stacked patch has a higher Q factor and the impedance is not stable versus frequency. In previous iterations of the antenna design this effect was worse. It has been partially mitigated by increasing the substrate height between the active and passive patch, increasing the antenna volume thereby lowering the Q factor. For both designs, a scanning angle of 45° is on the limit in terms of impedance match both in E-plane and H-plane. Three more elements were evaluated in the same way (not shown in this thesis) and the scanning limit was the same for all four elements.

3.4. Mutual Coupling

Energy from the excitation of an element in the array will radiate to neighbouring elements, inducing current on the patches and into the feed. Coupling is strongest towards direct neighbours in the array, and becomes weaker as the distance is increased. To quantify these coupling effects, for both antenna arrays the port coupling to a selection of elements with respect to a center element (4,4) is given in Figure 3.5. The port coupling is calculated only for Y-polarized (co-pol.) ports.

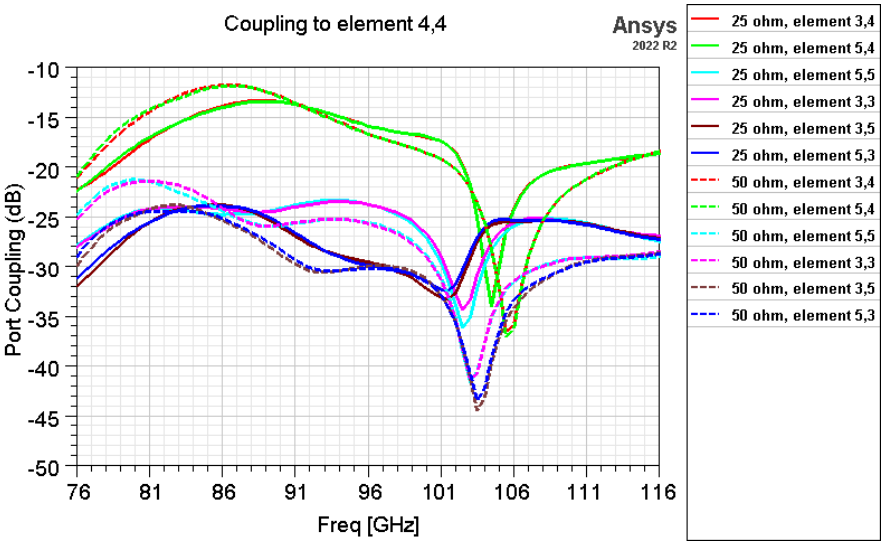

Figure 3.5: Port coupling between elements of the antenna array, 25 Ω (solid) and 50 Ω (dashed).

Both arrays show similar amounts of port coupling. Overall the 50 Ω array slightly outperforms the 25 Ω array by having lower amount of port coupling within the 20% bandwidth frequency range. It is

important to highlight the green and red curves, corresponding to the closest neighbouring elements. These show significant amounts of port-coupling. Comparing the 50 Ω and 25 Ω arrays, at the center frequency the closest neighbouring elements are coupled with -17 dB and -16 dB respectively. Both designs therefore do not meet the design requirement of -20 dB. Following this result, the propagation of electromagnetic fields on a cross-section of both arrays was analyzed. It was found that the cavity wall was visibly impenetrable for EM-waves. It seems that over-the-air coupling dominates the contribution for element-to-element coupling. Nevertheless, the port-coupling is acceptable since stability of the impedance is significantly improved by using cavity backed elements.

3.5. Radiation Performance

The radiation of both antenna arrays have been evaluated for a broadside beam and with a beam at the scanning limit ($\theta = 45°, \phi = 45°$). The radiation efficiency at the center frequency for a broadside beam is 92.18% for the 50 Ω array and 91.56% for the 25 Ω array. At the scanning limit the radiation efficiency is 94.77% for 50 Ω and 94.15% for 25 Ω. The gain of the antenna is also affected by scanning. Known as scan loss, the gain decreases as the beam is scanned away from broadside due to a reduction in aperture perpendicular to the beam direction. Intuitively this makes sense, as the gain of the antenna elements also maximises at broadside, and reduces when looking at angles away from broadside. For the 50 Ω and 25 Ω arrays, the peak gain of the main beam at broadside is 22.62 dBi and 22.61 dBi respectively. For a beam scanned at the scanning limit, the gain peaks at 20.97 dBi and 20.93 dBi respectively. The gain drops almost 2 dB due to scan loss in this case. Both antenna arrays have very similar antenna gain with the radiation efficiency being around 0.6% higher for the 50 Ω array.

Radiation patterns of the arrays are shown in Figure 3.6 for a broadside beam at 96 GHz. Both co- and cross-polarized patterns are shown in E- and H-plane. In Figure 3.7 the co-polarized patterns of both antenna designs are shown on the same plot, highlighting their differences.

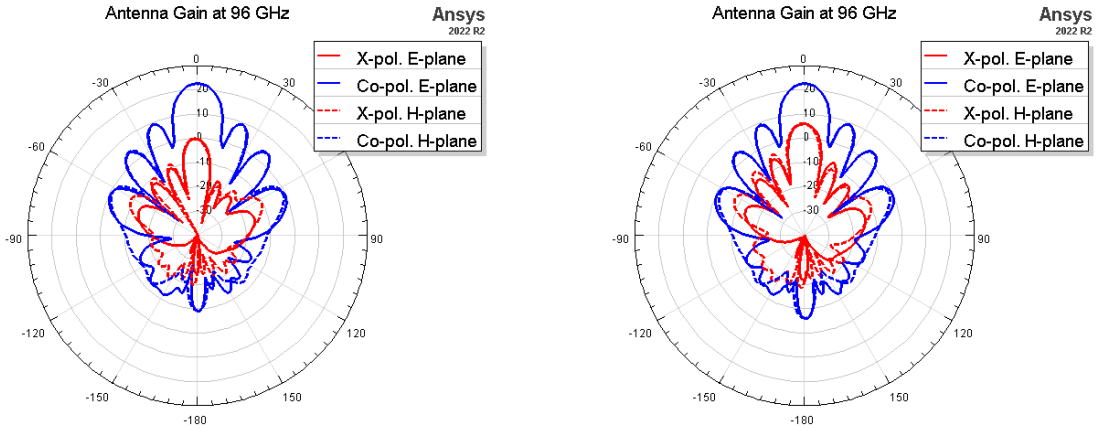

(a) 50 Ω reference design

(b) 25 Ω direct impedance matched design

Figure 3.6: Co-polarized (blue) and cross-polarized (red) patterns in E-plane (solid) and H-plane (dashed)

Similar to single element simulations from Chapter 2, the 25 Ω design has stronger cross-polarized radiation. X-pol levels in the broadside direction are around 4 dB higher with the first two sidelobes also showing significantly higher levels. The co-polarized radiation pattern is almost identical between both designs, both in E-plane and H-plane. One small difference is the back lobe, which is 4 dB stronger in the 25 Ω array. Despite using cavity walls which are supposed to suppress radiation in these directions and increase gain in the broadside direction[22].

When the beam is scanned to $\theta = 45°$ the main beam becomes less powerful due to scan loss, and the back- and sidelobes change significantly. The co-polarized 96 GHz radiation under these scanning conditions is shown in Figure 3.7.

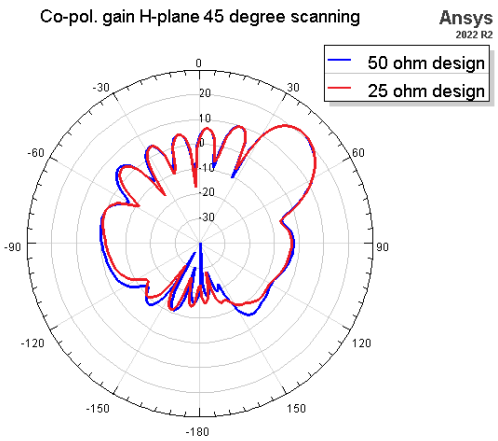

Figure 3.7: Co-polarized radiation at 96 GHz of both antenna arrays with 45° scanning

Because directivity is inversely related to beamwidth, the half-power beamwidth (HPBW) for both arrays at broadside is 13.5° while at a scanned angle it is 18°.

Sidelobe levels (SLL) of the highest sidelobe (relative to the main lobe) were found to be very similar for both arrays. Under broadside conditions, the SLL was -13.3 dB for both arrays. For a diagonally scanned observation ($\theta = 45°, \phi = 45°$) the SLL was -12.2 dB for the 50 Ω array and -11.6 dB for the 25 Ω array.

3.6. Conclusions

In this chapter, fundamental element designs were used to create 8x8 phased array antennas. A simulation approach has been explained to tackle the issue of long simulation times leading to a slow iterative design process. Infinite array simulations was fast option for simulations, but was deemed to be not accurate enough to design 8x8 arrays. Full finite array simulation had to be done for accurate results, for which Domain Decomposition Method (DDM) was used to increase parallelization of the computing process, lowering simulation time. Through an iterative process arrays were designed as reference (50 Ω) and as a novel direct impedance matched array (25 Ω). A comparison of impedance and bandwidth between both arrays found that the 25 Ω array is very similar to the 50 Ω reference. Both designs have similar amounts of variation of impedance between elements and feature comparable bandwidths. Input impedance was significantly affected by scanning. Scanning angles up to 45° in both E-plane and H-plane were possible in both arrays without mismatching the antenna above the -10 dB return loss threshold. Mutual coupling was visualized using port-to-port coupling data between neighbouring elements of a center element in the array. Again, both antennas show similar amounts of coupling between ports with the 50 Ω array slightly outperforming the 25 Ω array. Lastly, radiation performance was compared at the center frequency of 96 GHz. Compared to the 50 Ω reference design, the 25 Ω array had:

- Slightly lower radiation efficiency at broadside, 91.56% compared to 92.18%.
- Slightly lower radiation efficiency at the scanning limit, 94.15% compared to 94.77%.
- Nearly identical co-polarized gain of the main beam, both under broadside and scanned conditions.
- 4 dB higher backlobe radiation level.
- 4 dB higher cross-polarized radiation in broadside direction and for the first two sidelobes.
- Identical HPBW.
- Identical SLL under broadside conditions.
- Slightly higher SLL under scanned conditions, -11.6 dB compared to -12.2 dB.

In the next chapter, the antenna arrays are connected to an RF front-end circuit with a model of the power amplifier to assess the effects of direct impedance matching on system efficiency.

4

System Level Analysis

In this chapter, the antenna array designs from Chapter 3 are connected to a RF front-end circuit to simulate the antennas at a system level. Because this thesis aims to prove the merit of direct impedance matching for 6G phased arrays, the antenna is connected to a realistic model of a power amplifier. First, an overview of the system level simulation is given. Then, each part of the circuit is explained; the 1-tone AC signal source, 1-64 channel power divider, phase shifter and power amplifier. Simulation results are shown for both antenna arrays, after which a comparison is made.

4.1. RF Beamforming Circuit

To get a realistic impression of the performance of the antenna arrays a system level simulation was done using a FEM EM-model of the antenna arrays, co-simulated with a circuit simulation of RF front-end components. An overview of the beamforming circuit is given in Figure 4.1.

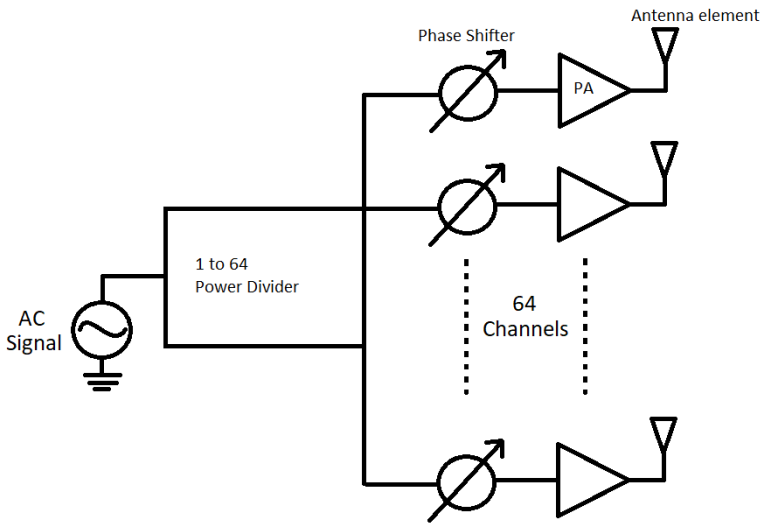

Figure 4.1: Schematic overview of RF beamforming circuit

4.1.1. Antenna Array

Simulations are done using Advanced Design System (ADS). In ADS the antenna designs from Chapter 3 were reproduced by defining a layer stack-up of package laminate substrate and copper conductor layers. Because ADS is a planar design tool, vertical components such as the cavity walls and feeding probes were modelled using conductor vias in the stack-up definition. Where HFSS provides the option

to add a radial wave-port to a cross section of coaxial line, this option is not available in ADS. Instead the wave-port excitation was reproduced by a combination of edge-pin voltage excitation, shown in Figure 4.2.

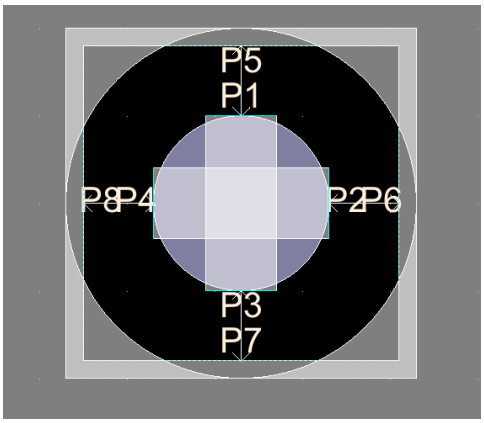

Figure 4.2: Reproduction of radial wave-port in ADS using pairs of edge-pins

The feeding probe and ground-plane at the ground-plane level were fitted with straight pieces of copper metal to provide surfaces for these edge-pins. P1-P4 were combined as the signal of the EM-port and P5-P8 were combined to be the ground reference. Since the coaxial lines below the antenna were de-embedded in HFSS simulations, this part of the feed was not modelled in ADS. Simulation results on the radiation and impedance of the antenna arrays in ADS matched the results from HFSS. Both the 25 Ω and 50 Ω antenna arrays were simulated at 96 GHz and EM-models were created with 64 EM-ports.

4.1.2. Power Amplifier

The power amplifier is a cascode amplifier in SiGe BiCMOS semiconductor technology. The amplifier draws power from a 2.4 V supply line and operates in class-A with a 2 mA bias current. Load-pull data of the PA (not shown in this thesis) indicate that for a fixed input signal, the output power of the amplifier maximises for a 25 Ω load. This motivated the design of the 25 Ω antenna array, such that it can be directly connected to the output of the PA.

Output Matching Network

To connect the 50 Ω antenna to the PA the impedance needs to be transformed from 50 Ω to 25 Ω to prevent voltage reflections at the PA-antenna interface. An L-network of a 70 fF series capacitor and a 80 pH parallel inductor is used. Both the capacitor and inductor are modeled as lossy components with a Q factor of 20 and 15 respectively. The Q-factor defines the ratio between the reactance and the internal resistance. For a capacitor, the Q-factor is given by:

$$Q_C = \frac{X_C}{R} = \frac{1}{\omega C R} \tag{4.1}$$

And for an inductor, the Q-factor is given by:

$$Q_L = \frac{X_L}{R} = \frac{\omega L}{R} \tag{4.2}$$

The Q-factors for the capacitor and inductor in the matching network were chosen to approximately represent the losses of realistic models of matching networks in SiGe IC design at 96 GHz. At this frequency, the matching network has an insertion loss of -0.5 dB, or 89% efficiency.

A test setup of the matching network is shown in Figure 4.3. An S-parameter analysis is done with a 25 Ω terminal, representing the PA output, into the matching network connected to a 50 Ω resistor, representing the antenna.

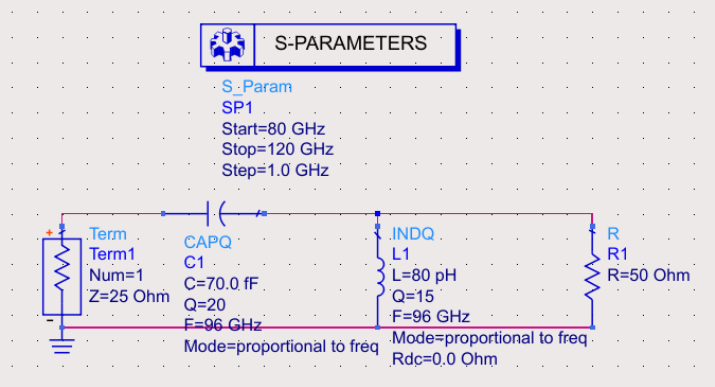

Figure 4.3: Test setup of the matching network

The input impedance and return loss of the matching network with a 50 Ω load is given in Figure 4.4. The impedance is 25 Ω at 96 GHz. It is very well matched over a large range of frequencies. The impedance bandwidth of the matching network far exceeds the bandwidth of the antenna.

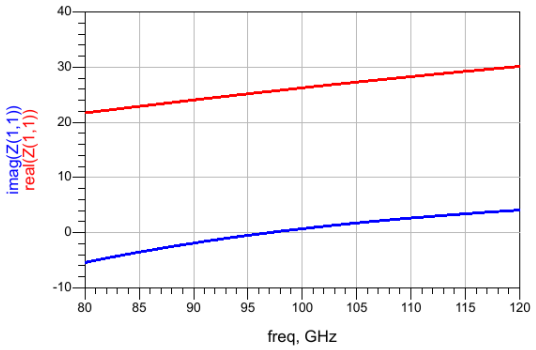

(a) Real and imaginary input impedance

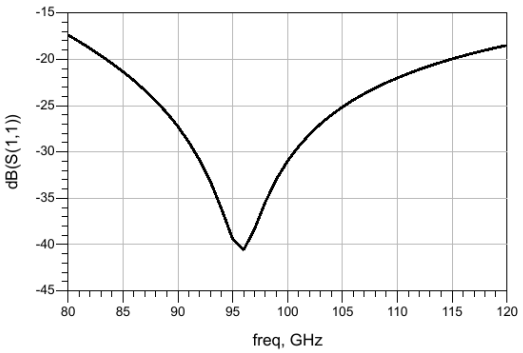

(b) Return loss

Figure 4.4: Simulation results of matching network with 50 Ω load

Internal resistances in the capacitor and inductor consume power, decreasing the efficiency of the network. In Figure 4.5 the efficiency is shown versus frequency. The efficiency was calculated using the insertion loss (S(2,1)) from the simulation. Between 92 and 100 GHz, the efficiency varies from 88.3% to 89.8% respectively, indicating a fairly consistent amount of losses.

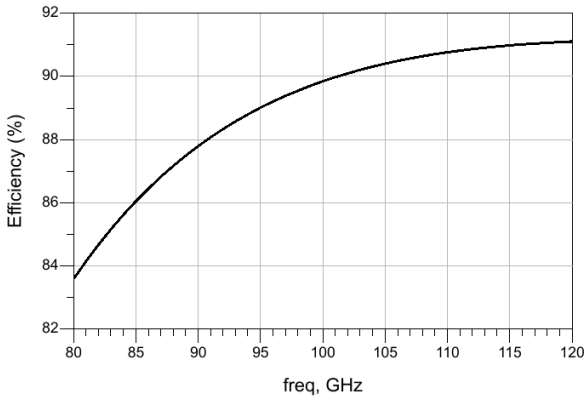

Figure 4.5: Efficiency of the matching network

4.1.3. Phase Shifter

The phase shifters in the simulation setup are ideal phase shifters with continuous phase shift control. The phase shifters of all 64 channels are given a phase shift according to equations 3.2 - 3.4. In reality, analogue phase shifters would be used that switch between delay lines of different lengths. This creates a set of discrete phase shifts, whereas the ideal phase shifter can use any phase shift. Realistic phase shifters also suffer from gain-phase error. For large phase shifts, the delay line is longer and more lossy which reduces the gain. This error can be compensated for with a Variable Gain Amplifier (VGA).

Note: Using the fourier transform relation between radiation pattern and amplitude distribution in the antenna aperture, a VGA can also be used for an amplitude tapering scheme (e.g. Chebyshev window) to reduce sidelobes, however this reduces antenna gain and increases beamwidth. To maximise the Effective Isotropic Radiated Power (EIRP), amplitude tapering is not used, and the VGA is not included in the RF circuit.

4.1.4. Power Divider

The power divider is modelled using ideal 2-way power splitters. These split the incoming signal into two signals with amplitude of $1/\sqrt{2}$ of the input, which exactly results in half the incoming power on each output. 2-way splits are done in 6 stages, resulting in $2^6 = 64$ channels. A realistic model of the power splitter, such as a 6 stage Wilkinson power divider, is not within the scope of this research.

4.2. Simulation Setup

To assess the performance of the beamforming system, radiation performance of EM-simulations are combined with efficiency results from circuit-simulations. To calculate the efficiency of the PA's, probes are added at the input, DC supply and output ports of the PA to measure the power. For the PA with output matching, the output power is measured after the matching network. Power Added Efficiency (PAE) of the amplifiers is calculated by:

$$PAE(\%) = 100 * \frac{P_{out} - P_{in}}{P_{DC}} \tag{4.3}$$

The reason the input power is taken into account in this calculation is because amplifiers can show very high efficiency at very low gain, painting a deceiving picture of the PA performance.

In addition to the PAE, AM/AM distortion and AM/PM distortion is also calculated. AM/AM shows the amplitude distortion between the input and the output of the PA and is dependent on the input power. When AM/AM is zero, the PA is linear. The linear region ends when AM/AM equals -1 dB, also known as the 1 dB compression point. AM/AM is calculated by:

$$AM/AM = G - G_0 \tag{4.4}$$

Where G_0 is the gain at the lowest simulated input power (where the amplifier is linear).

AM/PM distortion shows the phase modulation as a function of PA input power. Because amplitude tapering is not used, every channel has the same input power at each PA, thus any phase shift at a certain amount of input power will be equal for every channel and not have any effect. However, it is still useful to show the AM/PM distortion for each channel in broadside conditions, as this will show the difference in phase between in each channel due to load modulation.

To assess the system performance, it is important that the amplifiers are in the linear region with headroom for signal peaks. For this reason, the simulations are done at 6 dB below the 1 dB compression point. A broadside simulation with a power sweep on the AC source revealed the 1dB compression point, after which the simulations are done with the correct input power for linearity.

4.3. Results

A broadside simulation with no phase shift was done for both antenna arrays. The 25 Ω array had its elements directly connected to the power amplifier. The 50 Ω array had an impedance matching

network between each of the 64 PA's and antenna elements. Average power of the AC source was swept from 10 dBm to 30 dBm. This power is split evenly into 64 channels, reducing the power by around 18.06 dB, such that the input power of the PA in each channel ranges between -8 dBm and 12 dBm. PAE of each channel for both 25 Ω and 50 Ω antennas is shown in Figure 4.6.

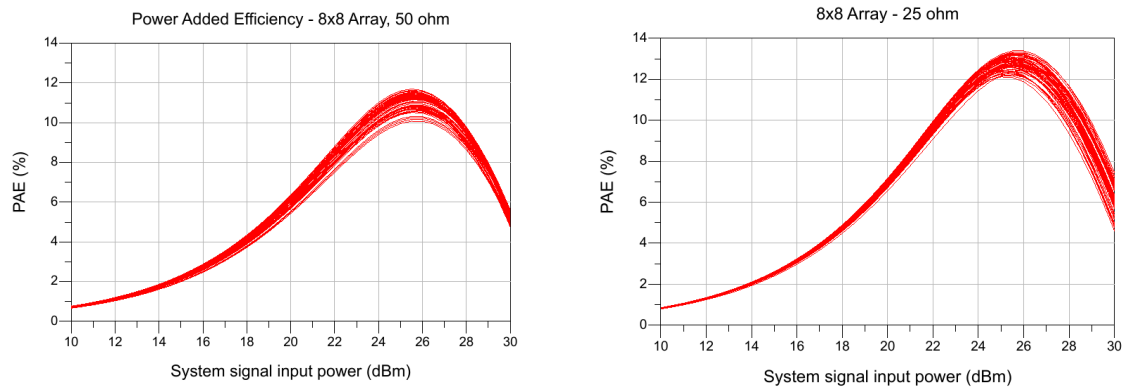

(a) 50 Ω antenna with matching network

(b) 25 Ω direct impedance matched antenna

Figure 4.6: PAE of all channels at 96 GHz and broadside beam

PAE peaks between 25 dBm and 26 dBm AC source power, depending on the channel. The peak PAE of the 25 Ω array is higher by around 1.5 percent points and shows less variation between the channels. To visualize the relative increase in amplifier PAE between the 25 Ω and 50 Ω antennas, three channels were selected and compared in Figure 4.7. Channel 1 corresponds to the corner element (1,1), channel 13 to side element (2,4) and channel 28 to center element (4,4).

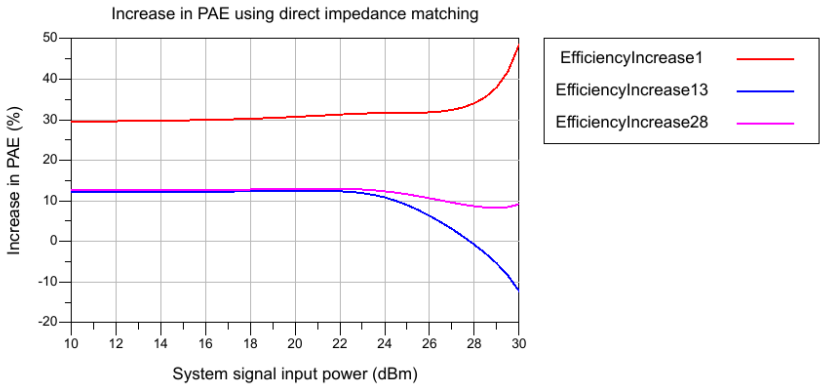

Figure 4.7: Percentage increase of PAE when using direct impedance matched antenna, three channels shown

Figure 4.7 shows the increase in efficiency is consistent as long as the amplifier is operating in the linear region. On the other hand, the efficiency increase is not consistent throughout the array. The corner element in this case gains significantly more efficiency than the side and center element. This is most likely caused by higher load modulation in the 50 Ω antenna array, meaning that elements in the array have more variance in their impedance, as is evident by the larger spread of PAE in Figure 4.6a. Moreover, the four lowest curves in Figure 4.6a correspond to all of the corner elements, indicating a large impedance mismatch.

AM/AM distortion for both antenna arrays is shown in Figure 4.8. In both cases, the 1 dB compression point occurs around 24 dBm of AC source power, or 6 dBm of input power at each channel. To assess the performance of the system, 6 dB of headroom is given to the 1 dB compression point, so the power of the AC source is set to 18 dBm resulting in roughly 1 mW of input power at each channel.

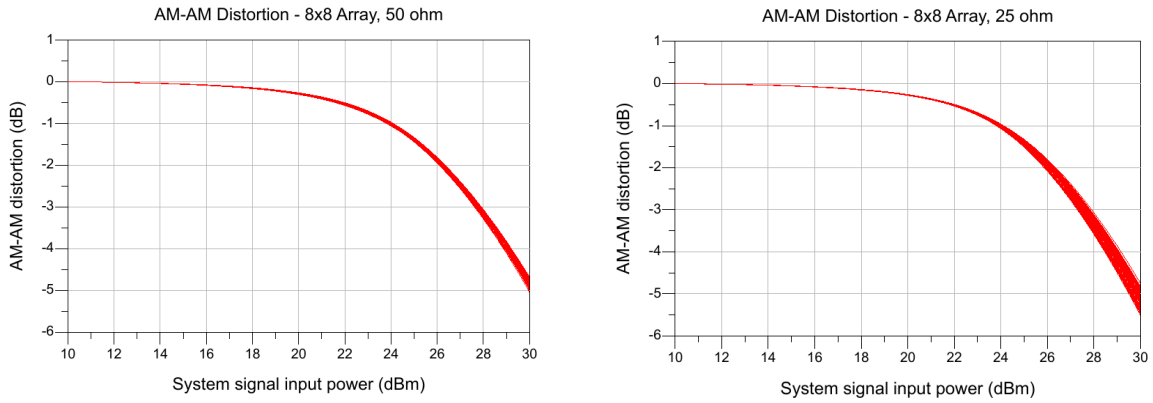

(a) 50 Ω antenna with matching network

(b) 25 Ω direct impedance matched antenna

Figure 4.8: AM/AM distortion of all channels at 96 GHz and broadside beam

AM/PM distortion is shown for broadside conditions in Figure 4.9. Ideally, the phase between channels should be equal since there is no beam steering from the phase shifters at broadside. Instead, there is spread in the phase between channels. Comparing the 50 Ω and 25 Ω results, the maximum spread is around 7.4° and 10.8° respectively. The 25 Ω antenna likely has larger phase spread due to a higher spread in imaginary impedance relative to the characteristic impedance. In terms of absolute phase there is a substantial difference in phase between both arrays, though this does not affect the performance.

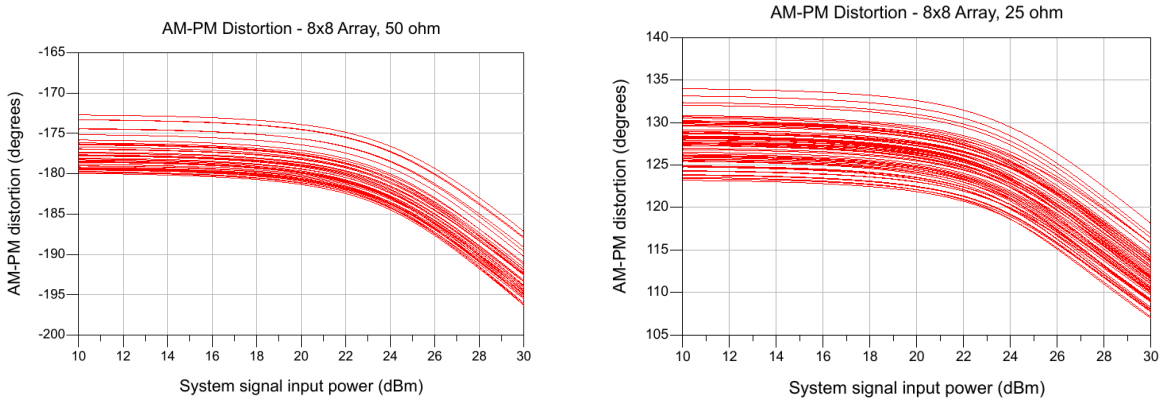

(a) 50 Ω antenna with matching network

(b) 25 Ω direct impedance matched antenna

Figure 4.9: AM/PM distortion of all channels at 96 GHz and broadside beam

To get a complete impression of the PA-antenna performance, the input-, DC supply- and output powers are added over all the channels. This allows for calculation of the total PAE of the PA-antenna:

$$PAE_{total}(\%) = 100 * \frac{P_{out,total} - P_{in,total}}{P_{DC,total}} * \mu \tag{4.5}$$

where μ is the radiation efficiency of the antenna array. In addition to this, the power output of the antenna radiation in the direction of the main beam is represented by the EIRP, calculated by:

$$EIRP = P_{out,total} * G_{array} \tag{4.6}$$

Because the antenna is directly connected to the PA module in the circuit, output power over all channels is the same as the input power of the array. For this reason it can be used to calculate the EIRP,

where the total output power already includes mismatch losses and the gain of the array is the product of the directivity and radiation efficiency.

Both antenna arrays are now simulated at 96 GHz under broadside condition and diagonally scanned condition ($\theta = 45°, \phi = 45°$) with 6 dB headroom to the 1 dB compression point. Results were obtained on the radiation, power output and efficiency of the system, shown in Table 4.1.

Table 4.1: System simulation results for 18 dBm AC source power at 96 GHz

Parameters	Broadside Beam		Scanned Beam ($\theta = 45°, \phi = 45°$)	
Antenna Impedance	50 Ω	25 Ω	50 Ω	25 Ω
Radiation Efficiency	92.18%	91.56%	94.77%	94.15%
Peak Gain	22.62 dB	22.61 dB	20.97 dB	20.93 dB
HPBW	13.5°	13.5°	18°	18°
Antenna Input Power	275 mW	310 mW	249 mW	306 mW
EIRP	50.30 W	56.32 W	31.12 W	37.86 W
PA Total PAE	4.1%	4.77%	3.58%	4.69%
PA PAE spread	3.73 - 4.36%	4.50 - 4.91%	2.83 - 4.07%	3.87 - 5.25%
PA+Antenna Total PAE	3.78%	4.37%	3.39%	4.42%
Max Phase Error Between Channels	7.4°	10.8°	N/A	N/A

4.4. Conclusions

In this chapter, a novel 8x8 antenna array with direct impedance matching at 25 Ω was compared with a reference array at 50 Ω. The antenna arrays were co-simulated with an RF-circuit in ADS. The circuit comprised of an AC signal source, an ideal 1-64 channel power divider, ideal continuous phase shifters and realistic SiGe Class A cascode PA models. The 25 Ω array was directly connected to the PA's and the 50 Ω array was connected with a lossy matching network in between. The matching network was made using a 70 fF series capacitor and an 80 pH parallel inductor with Q factor of 20 and 15 respectively. At 96 GHz, 11% of the power from the PA output is dissipated in the matching network.

To simulate the antenna arrays properly, a simulation at broadside with a sweep on the input signal power was done to find the 1 dB compression point of the PA. The PA was found to be linear up to 24 dBm of average AC source power. 6 dB of headroom to the 1 dB compression point was given for a realistic simulation, putting the AC source average power at 18 dBm, or roughly 1 mW per channel. This simulation was done for a broadside beam and a diagonally scanned beam at ($\theta = 45°, \phi = 45°$). PAE and phase modulation showed significant spread between channels due to impedance spread among elements in the antenna arrays. Both antenna arrays had comparable gain, but because the input power to the 25 Ω array was considerably higher than the 50 Ω reference, the EIRP was also higher.

To conclude, the power is higher in the 25 Ω antenna system due to a better PAE. Comparing the PAE of the 25 Ω antenna system with the 50 Ω reference, the efficiency improves by 15.6% with a broadside beam and 30.4% with a scanned beam ($\theta = 45°, \phi = 45°$).

5

Conclusion and Future Research

5.1. Conclusion

The goal of this thesis was to show the merit of an antenna array design with direct impedance matching for a 6G beamforming RF-IC. To show this, a 25 Ω antenna array was designed to match the PA output impedance directly. This array was then compared with a reference antenna array of 50 Ω. The comparison was a trade-off study between radiation performance and power efficiency. This study was structured into four major parts. First an extensive literature study was done to assess the current state of direct impedance matched antennas. Then a unit cell antenna element was designed for 25 Ω and compared to a 50 Ω reference design. With additional tuning, 8x8 antenna arrays were designed using the unit cells as a basis. Again a comparison was done, focusing on impedance, bandwidth and radiation patterns. To complete the research, both array designs compared using a circuit-EM co-simulation. Here the 50 Ω antenna array was connected to power amplifiers with a matching network in between, whereas the 25 Ω array was directly connected to the PA's. The RF systems were compared in terms of radiation performance and power efficiency.

Based on the literature study, direct impedance matching has been shown to be a method for increasing PAE in RF systems. This leads to a higher radiated power, increasing wireless link quality. Moreover, by increasing the efficiency, less heat is generated on the RF-IC which is significant for antenna-in-package systems where high integration leads to very closely spaced components. Examples of direct impedance matched antennas found in literature vary in design type and frequency, with most designs featuring a single radiating element. Only two studies investigated direct impedance matching for an antenna array, but both featured a fixed linear array configuration without beam-steering. **This thesis presents a novel 8x8 planar antenna array design using a cavity backed pin-fed dual-polarized stacked patch antenna. The antenna array, with an impedance of 25 Ω, is directly matched to the impedance of the power amplifiers. In addition, the antenna design is compatible with Antenna-in-Package technology. For the first time, direct impedance matching has been demonstrated in a phased array using a circuit-EM co-simulation featuring controllable phase shifters and realistic power amplifier models.**

The initial design of the unit cell antennas started with a basic square probe-fed patch antenna. Bandwidth of this antenna was found to be too low, thus broadbanding techniques were required. Because the design is constrained due to limited size of the antenna element for use in arrays, and due to dual polarization forcing the antenna to be the same along both X- and Y axes, the stacked patch antenna was found to be a good solution for extending the bandwidth. The problem of probe reactance was identified and different solutions were investigated. By reducing the height of the bottom substrate, the probe shortens and reactance is reduced. This was found to be the most effective method of achieving a real 25 Ω antenna impedance. To make this impedance more stable for use in arrays, via walls around the perimeter of the element were added to act as a cavity. Comparing the 25 Ω antenna to the 50 Ω reference antenna it had lower bandwidth, radiation efficiency and gain. Cross-polarization levels were also 4 dB higher in the 25 Ω antenna.

Based on these designs, 8x8 antenna arrays were designed. Both the 25 Ω and 50 Ω array feature cavity-backed elements and follow the same design principals (probe-fed dual-polarized stacked patch). Both arrays have identical dimensions and are built on the same substrate stack-up. For accurate design and modelling of these arrays, full finite array simulations were done in HFSS using Domain Decomposition Method (DDM) to increase parallelization of the computing process. Comparing the 25 Ω antenna array to the 50 Ω reference array the bandwidth, impedance variance, co-polarized gain, SLL and maximum scanning angle is similar. Radiation efficiency was slightly lower in the 25 Ω array, although the difference is less than 1%. The most notable difference was the level of cross-polarized radiation and backlobe radiation, both being 4 dB higher in the 25 Ω array. These results show that by going to a lower impedance in this antenna design, its performance does not suffer significantly.

Using ADS, the antenna arrays were co-simulated with an RF-circuit. An AC signal source, ideal 1-64 channel power divider, ideal continuous phase shifters and realistic SiGe Class A cascode PA models were all connected to EM models of the antenna arrays. coaxial waveguide ports were imitated in ADS by introducing flat edges to the feeding probe and ground plane hole. Voltage pins were connected along these edges and were combined into EM ports. The 25 Ω array had a direct connection between its elements and the PA's. For the 50 Ω array, an impedance matching network using a 70 fF series capacitor and a 80 pH parallel inductor was put in between. The matching network dissipates 11% of the power at 96 GHz. The RF-circuit was simulated such that the PA's operate at 6 dB below the 1 dB compression point. Both arrays showed variance in the PAE and phase modulation in each channel. **In the 25 Ω array, direct impedance matching led to an increase in PAE of 15.6% at broadside conditions and 30.4% with a scanned beam ($\theta = 45°, \phi = 45°$)**. Gain of both arrays was comparable, but the 25 Ω array radiated more power, leading to a higher EIRP.

Although outside of the scope of this thesis, the feeding network can also greatly benefit from a lower characteristic impedance. By going from a 50 Ω to a 25 Ω coaxial line, the radius of the outer conductor is more than halved. Because the array elements are dual polarized and closely spaced (half-wavelength spacing), routing the antenna ports through the package laminate to the IC becomes far easier with more compact feeding lines.

To sum up, by using a direct impedance matching approach, the drawbacks of higher cross polarized- and backlobe radiation are outweighed by significant increase in radiated power and efficiency. This makes direct impedance matching a good design strategy for 6G beamforming AiP technology.

5.2. Recommendations for Future Research

Direct impedance matching has been shown to increase efficiency and radiated power in 6G RF-IC phased array AiP's. The radiation characteristics of this novel antenna design is comparable to state-of-the-art antenna arrays. Despite this, there are still ways to improve and extend this research. In this final section of the thesis an evaluation of this work is given along with proposals for future research.

- **Optimization of proposed antenna array designs:** The designs for 25 Ω and 50 Ω antenna arrays presented in this work are not fully optimized. There is still room for improvement in terms of impedance matching, where fine tuning can lead to the antenna impedance being closer to the design impedance (25 Ω and 50 Ω). Due to the iterative design process being slow with long simulation time, further optimization was not done in this work. Changing the substrate heights in both layers, as well as further tuning with patch sizes and feed positions, a better performing antenna array is likely to exist. In addition, there are also options to explore other impedances with direct impedance matching benefits, this depends on the PA design that is used.
- **Accurate package laminate material model:** In this work, the package laminate was modelled as a dielectric with a permittivity of 3.35 and a loss tangent of 0.0055. These characteristics were obtained from measurements at 10 GHz, but the antenna is designed at 96 GHz. The behaviour of the laminate material is not expected to be the same at 10x the frequency. Due to a lack of information, the 10 GHz data was used, which would still give a fair comparison between both antenna designs in this work. For a more complete picture of the antenna performance however, material characteristics at 100 GHz would be needed. This would probably lead to lower radiation efficiency in both designs, as substrate laminates are typically more lossy at high frequency.
- **Broadband radiation performance simulation:** Due to constraints on the data size of the EM-

model for compatibility with the circuit co-simulation, RF system performance was only simulated with a single tone at 96 GHz. Additional simulations at other frequencies, such as 92 GHz and 100 GHz, would give insight in the frequency dependence of the system. Additionally, a simulation can be done with a wideband signal source.

- **Address cross-polarized radiation:** In this work, cross-polarized radiation was not specifically addressed. Wideband dual-polarized patch antennas with low cross-polarization levels have been shown in [24]. As a future work, compatibility of these methods with AiP technology and direct impedance matching could be investigated.
- **Address array edge effects using dummy elements:** To overcome the challenge of large variation between array elements, dummy element layers can be added around the perimeter of the active array. These elements are connected to matched loads and simply serve as passive neighbours to reduce edge effects of the outer active elements. In this work, dummy elements were not used, thereby keeping simulation time and data size within practical amounts. An 8x8 array with a single dummy layer (making it 10x10) was not compatible with the circuit-EM co-simulation in this work due to file size exceeding the limits. By using more computing resources or with a more efficient simulation method, dummy elements can still be explored.
- **Extend accuracy of system simulation with additional real components:** In this work, only the power amplifiers and antennas were modelled as realistic components. The phase shifters and power dividers were all modelled as ideal components, and thus had no errors or losses. Moreover, the feeding network between the PA's and antenna ports was completely omitted from the model. For a more realistic representation of the system performance, a feeding network model should be added, along with realistic N-bit phase shifters and Wilkinson power divider. Phase gain errors of the phase shifters can be compensated using variable gain amplifiers (VGA's). Each block can be modelled using its S-parameters, which gives insight in the losses and reflections of the RF signal.
- **Reduce SLL with amplitude tapering:** Aforementioned VGA's can also be used to taper the signal amplitude distribution in the array such that SLL is reduced. Tapering schemes such as a Chebyshev window can be used to reduce the side lobes to any desired level, although at the cost of directivity of the main beam.
- **Study the impact of cavity backed array elements:** In this work the impact of cavity backing was briefly compared in Appendix A, showing advantages and drawbacks of this technique. Impedance was found to be more stable under scanned conditions with cavity walls in place, but numerical results from the system level simulation showed better performance from the 50 Ω array without cavities under scanned conditions. In addition, the cavity backed array showed higher levels of element-to-element port coupling. These effects could be studied closer to get a better understanding of the impact of cavity backing, along with design strategies for implementing this technique.

References

[1] Yueping Zhang and Junfa Mao. “An Overview of the Development of Antenna-in-Package Technology for Highly Integrated Wireless Devices”. In: *Proceedings of the IEEE* 107.11 (2019), pp. 2265–2280. DOI: 10.1109/JPROC.2019.2933267.

[2] Yanki Aslan et al. “Thermal-Aware Synthesis of 5G Base Station Antenna Arrays: An Overview and a Sparsity-Based Approach”. In: *IEEE Access* 6 (2018), pp. 58868–58882. DOI: 10.1109/ACCESS.2018.2873977.

[3] Yanki Aslan et al. “Passive Cooling of mm-Wave Active Integrated 5G Base Station Antennas Using CPU Heatsinks”. In: *2019 16th European Radar Conference (EuRAD)*. 2019, pp. 121–124.

[4] Peter Song et al. “W-band SiGe power amplifiers”. In: *2014 IEEE Bipolar/BiCMOS Circuits and Technology Meeting (BCTM)*. 2014, pp. 151–154. DOI: 10.1109/BCTM.2014.6981303.

[5] Wooram Lee et al. “Fully Integrated 94-GHz Dual-Polarized TX and RX Phased Array Chipset in SiGe BiCMOS Operating up to 105 °C”. In: *IEEE Journal of Solid-State Circuits* 53.9 (2018), pp. 2512–2531. DOI: 10.1109/JSSC.2018.2856254.

[6] Andrew Townley et al. “A 94GHz 4TX-4RX phased-array for FMCW radar with integrated LO and flip-chip antenna package”. In: *2016 IEEE Radio Frequency Integrated Circuits Symposium (RFIC)*. 2016, pp. 294–297. DOI: 10.1109/RFIC.2016.7508309.

[7] Martijn de Kok et al. “A Review of PA-Antenna Co-design: Direct Matching, Harmonic Tuning and Power Combining”. In: *2022 52nd European Microwave Conference (EuMC)*. 2022, pp. 536–539. DOI: 10.23919/EuMC54642.2022.9924344.

[8] Essia Ben Abdallah et al. “Impact of small antenna on linear power amplifier performance in a co-design approach”. In: *2015 IEEE 13th International New Circuits and Systems Conference (NEWCAS)*. 2015, pp. 1–4. DOI: 10.1109/NEWCAS.2015.7181998.

[9] Wan-Chun Liao et al. “A Ka-Band Active Integrated Antenna for 5G Applications: Initial Design Flow”. In: *2018 2nd URSI Atlantic Radio Science Meeting (AT-RASC)*. 2018, pp. 1–4. DOI: 10.23919/URSI-AT-RASC.2018.8471330.

[10] Wan-Chun Liao et al. “A Directly Matched PA-Integrated K-Band Antenna for Efficient mm-Wave High-Power Generation”. In: *IEEE Antennas and Wireless Propagation Letters* 18.11 (2019), pp. 2389–2393. DOI: 10.1109/LAWP.2019.2937235.

[11] Srinaga Nikhil Nallandhigal and Ke Wu. “Unified and Integrated Circuit Antenna in Front End—A Proof of Concept”. In: *IEEE Transactions on Microwave Theory and Techniques* 67.1 (2019), pp. 347–364. DOI: 10.1109/TMTT.2018.2872962.

[12] Hyungrak Kim, Ick-Jae Yoon, and Young Joong Yoon. “A novel fully integrated transmitter front-end with high power-added efficiency”. In: *IEEE Transactions on Microwave Theory and Techniques* 53.10 (2005), pp. 3206–3214. DOI: 10.1109/TMTT.2005.855142.

[13] Arpan Pal et al. “Co-design of an antenna-power amplifier RF front-end block without matching network for 2.4 GHz WiFi application”. In: *2017 IEEE Radio and Wireless Symposium (RWS)*. 2017, pp. 201–203. DOI: 10.1109/RWS.2017.7885987.

[14] Yunlong Lu et al. “Seamless Integration of Active Antenna With Improved Power Efficiency”. In: *IEEE Access* 8 (2020), pp. 48399–48407. DOI: 10.1109/ACCESS.2020.2978906.

[15] Constantine Balanis. *Antenna Theory: Analysis and Design*. Vol. 1. Apr. 2005. ISBN: 047166782X , 978-0471667827.

[16] Vasiliki K. Paraforou. “Design and full-wave analysis of supershaped patch antennas”. In: 2013. URL: https://api.semanticscholar.org/CorpusID:108066040.

[17] Tomas Mikulasek et al. “Transverse slot with control of amplitude and phase for travelling-wave SIW antenna arrays”. In: *IET Microwaves, Antennas Propagation* 14 (Oct. 2020), pp. 1943–1946. DOI: 10.1049/iet-map.2020.0069.

[18] S. Long and M. Walton. “A dual-frequency stacked circular-disc antenna”. In: *IEEE Transactions on Antennas and Propagation* 27.2 (1979), pp. 270–273. DOI: 10.1109/TAP.1979.1142078.

[19] R.B. Waterhouse. “Design of probe-fed stack patches”. In: *Antennas and Propagation, IEEE Transactions on* 47 (Jan. 2000), pp. 1780–1784. DOI: 10.1109/8.817653.

[20] Mohammad Fakharian et al. “A Capacitive Fed Microstrip Patch Antenna with Air Gap for Wideband Applications”. In: *International Journal of Engineering, Transactions B: Applications* 27 (May 2014). DOI: 10.5829/idosi.ije.2014.27.05b.06.

[21] F. Zavosh and J.T. Aberle. “Improving the performance of microstrip-patch antennas”. In: *IEEE Antennas and Propagation Magazine* 38.4 (1996), pp. 7–12. DOI: 10.1109/74.537361.

[22] Anil Kumar Singh et al. “Effect of cylindrical cavity enclosure on resonance frequency of annular ring microstrip antenna”. In: *2013 International Conference on Microwave and Photonics (ICMAP)*. 2013, pp. 1–3. DOI: 10.1109/ICMAP.2013.6733507.

[23] Ioan E. Lager and Massimiliano Simeoni. “Experimental investigation of the mutual coupling reduction by means of cavity enclosure of patch antennas”. In: *2006 First European Conference on Antennas and Propagation*. 2006, pp. 1–5. DOI: 10.1109/EUCAP.2006.4584577.

[24] Biao Li et al. “Wideband Dual-Polarized Patch Antenna With Low Cross Polarization and High Isolation”. In: *IEEE Antennas and Wireless Propagation Letters* 11 (2012), pp. 427–430. DOI: 10.1109/LAWP.2012.2195149.

A

8x8 Cavity Backed Array Comparison

This section contains a comparison between a cavity backed 50 Ω antenna array and a 50 Ω array without cavities. The comparison covers antenna impedance, bandwidth, radiation performance and coupling effects.

Dimensions of the compared arrays are given in table A.1.

Table A.1: Dimensions of both antenna array designs

Patch Antenna Parameters		50 Ω cavity	50 Ω no cavity
f_0	Center Frequency	96 GHz	96 GHz
ϵ_r	Substrate Dielectric Permittivity	3.35	3.35
h_1	Bottom Substrate Thickness	0.125 mm	0.14 mm
h_2	Top Substrate Thickness	0.21 mm	0.21 mm
$W_1 = L_1$	Active Patch Length and Width	0.70 mm	0.70 mm
$W_2 = L_2$	Passive Patch Length and Width	0.66 mm	0.62 mm
D_{probe}	Diameter of Probe Feed	0.10 mm	0.087 mm
D_{ground}	Diameter of Ground Hole	0.20 mm	0.20 mm
y_0	Inset Feed Position	0.09 mm	0.09 mm
t_m	Microstrip Metal Thickness	15 µm	15 µm
$W_s = L_s$	Substrate Length and Width	12 mm	12 mm

The antenna impedance of a center element as function of scanning angle in H-plane and E-plane is given on the Smith chart in Figures A.1 and A.2 respectively. The antenna impedance is more stable around the 50 Ω mark in the cavity backed array allowing for larger scanning range of the array without severe mismatch losses. Under broadside beamforming conditions, the -10 dB bandwidth is 18 GHz for the cavity backed array and 16 GHz for the array without cavities.

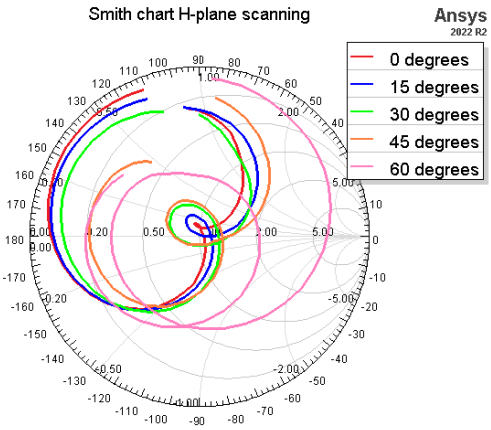

(a) 50 Ω cavity backed

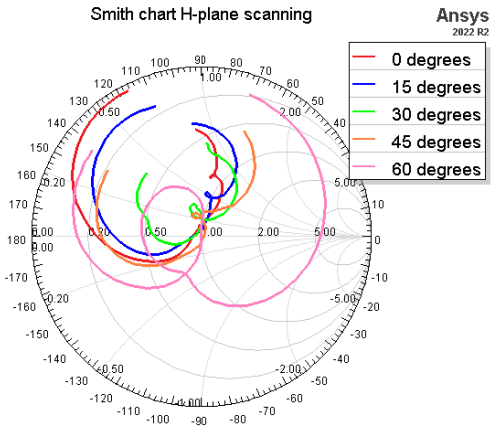

(b) 50 Ω without cavities

Figure A.1: Impedance of center element (4,4) vs scanning angles $0°$ to $60°$ in H-plane

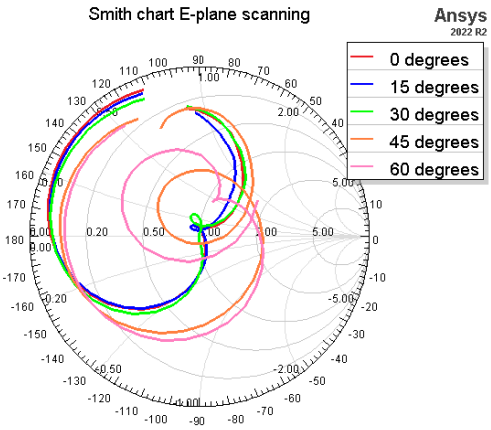

(a) 50 Ω cavity backed array

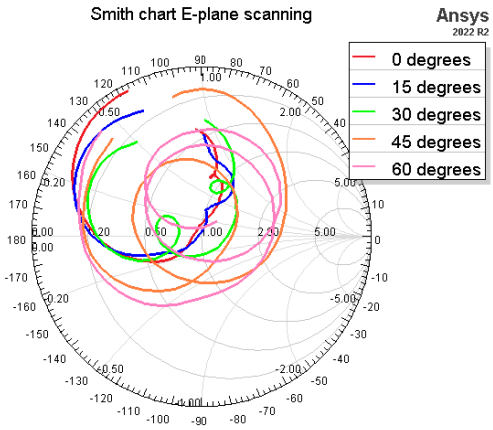

(b) 50 Ω array without cavities

Figure A.2: Impedance of center element (4,4) vs scanning angles $0°$ to $60°$ in E-plane

At 96 GHz, radiation efficiency for the cavity backed array and the array without walls is 94.0% and 98.3% respectively. Radiation patterns of both arrays are shown in Figure A.3. The cavity backed array has cross-polarization levels -3 dB lower compared to the array without cavity walls.

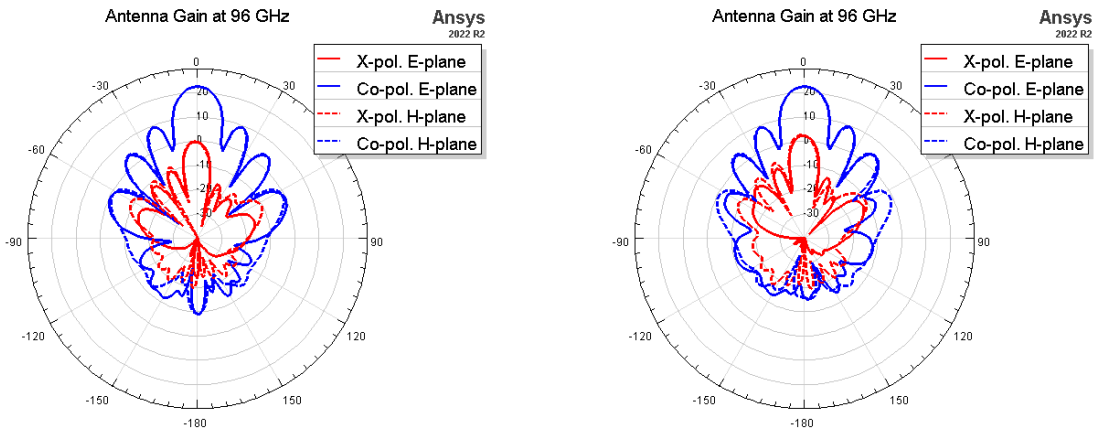

(a) 50 Ω cavity backed array

(b) 50 Ω without cavities

Figure A.3: Co-polarized (blue) and cross-polarized (red) patterns in E-plane (solid) and H-plane (dashed)

The cross-polarized power in the direction of the main beam is thus halved by adding cavities on the antenna elements. Co-polarized gain of the main beam is identical in both arrays.

Port coupling is shown in Figure A.4. The coupling of a selection of elements is given with respect to the center element (4,4) for both arrays.

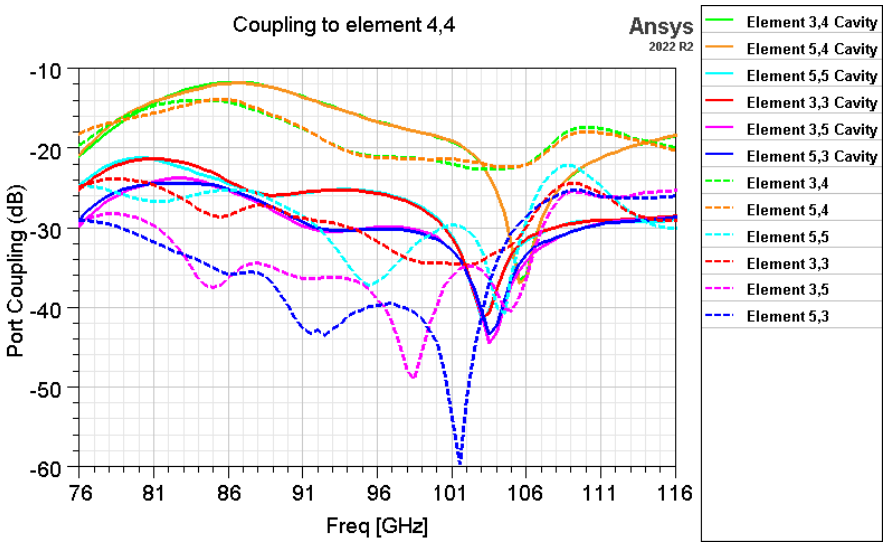

Figure A.4: Port coupling between antenna elements in the cavity backed array (solid) and the array without cavities (dashed)

Although the walls of the cavities should lead to higher isolation between elements, port coupling is significantly higher in the cavity backed array. Cross-sections of the array revealed no propagation of EM fields through the wall structures, suggesting the cause is due to stronger over-the-air coupling.

The 50 Ω array **without cavities** was also compared to the 25 Ω cavity backed design using the setup from Chapter 4. In Table A.2 the results are summarized.

Table A.2: System simulation results for 18 dBm AC source power at 96 GHz

Parameters	Broadside Beam		Scanned Beam ($\theta = 45°, \phi = 45°$)	
Antenna Impedance	50 Ω	25 Ω	50 Ω	25 Ω
Radiation Efficiency	94.29%	91.56%	95.64%	94.15%
Peak Gain	22.68 dB	22.61 dB	20.84 dB	20.93 dB
HPBW	13.5°	13.5°	18°	18°
Antenna Input Power	271 mW	310 mW	280 mW	306 mW
EIRP	49.24 W	56.32 W	34.00 W	37.86 W
PA Total PAE	4.03%	4.77%	4.20%	4.69%
PA PAE spread	3.69 - 4.37%	4.50 - 4.91%	3.38 - 5.54%	3.87 - 5.25%
PA+Antenna Total PAE	3.80%	4.37%	4.02%	4.42%
Max Phase Error Between Channels	7.4°	10.8°	N/A	N/A

In this case, compared to the results of the 50 Ω antenna with cavities (see Table 4.1), the benchmark antenna without cavities performs better under scanned conditions. The total system is more efficient and radiates more power. Nevertheless, these results are only for 96 GHz. It is possible that other frequencies within the bandwidth of operation perform worse due to larger mismatching, shown by the impedance stability in Figures A.2 and A.1.